2009

Acoustic plethysmograph for measuring pulmonary function in mice

Jeffrey S. Reynolds
West Virginia University

Acoustic Plethysmograph for Measuring Pulmonary Function in Mice

Jeffrey S. Reynolds

Dissertation submitted to the
College of Engineering and Mineral Resources
at West Virginia University
in partial fulfillment of the requirements
for the degree of

Doctor of Philosophy
in
Electrical Engineering

Wils Cooley, Ph.D., Chair
David Frazer, Ph.D.
Mark Jerabek, Ph.D.
Xin Li, Ph.D.
William Lindsley, Ph.D.

Lane Department of Computer Science and Electrical Engineering

Morgantown, West Virginia
2009

Keywords: specific airway resistance, Helmholtz resonator, unrestrained plethysmograph, whole-body plethysmograph, acoustic plethysmograph.

Acoustic plethysmograph for measuring pulmonary function in mice

Jeffrey S. Reynolds

Abstract

The traditional whole body plethysmograph (WBP) relies on pressure changes induced by a freely respiring animal inside a chamber. This pressure is a combination of a thermo-hygrometric effect (proportional to tidal volume) and a gas compression effect (related to lung mechanics). In order to measure either tidal volume or lung mechanics, it must be assumed that the other component is negligible. In this research, an acoustic WBP was developed that is capable of measuring the thoracic volume change of a mouse independent of the thermo-hygrometric effect. This allows independent measurement of tidal volume and specific airway resistance.

In the first phase of this research, the plethysmograph was designed to optimize measurement of the acoustic signal, which involved minimizing the WBP pressure. This plethysmograph was designed as a resonating cavity at a fixed frequency. It had a sharp resonant peak and was tuned so that changes in body volume produced nearly linear changes in sound amplitude. The plethysmograph was tested with a water filled balloon connected to a syringe pump. The volume of the balloon was varied as a triangle wave with amplitude of 250 μL. The RMS error between measured and delivered volume was 4.43 μL. A volume step test, performed to assess the response time of the system, showed that the plethysmograph responded in less than one millisecond.

Next, the plethysmograph was redesigned to provide a compromise between the acoustic measurement and the WBP pressure measurement. Similar to traditional methods utilizing a double chamber plethysmograph, these measurements were combined to estimate specific airway resistance (sRaw). To evaluate the system, six conscious A/J mice were individually placed in a chamber for a two-minute exposure to aerosolized methacholine chloride dissolved in saline (0, 5, 10, and 20 mg/mL) which is known to increase sRaw in mice. Following exposure, the mice were transferred to the acoustic plethysmograph for data collection. The mean baseline value of sRaw was $0.93 \pm 0.10\ cm\ H_2O \cdot sec$. A dose-dependent increase in sRaw was shown, with an approximate tripling of sRaw at the highest dose. These results are comparable to those of other methods reported in the literature.

key terms: specific airway resistance, Helmholtz resonator, unrestrained plethysmograph, whole-body plethysmograph, acoustic plethysmograph.

Acknowledgments

I would like to thank my friend and mentor Dr. Dave Frazer. This pursuit would likely have never been initiated without his encouragement and guidance. I hope we have many more days together both at work and on the golf course.

I would also like to thank my committee for their patience and help. A special thanks goes to my advisor, Dr. Wils Cooley, for sticking with me even into his retirement.

I would like to express my gratitude to my wife, Elizabeth, and our children, Jacob, Katherine, Julia, and Caroline, who all put up with my grumpy moods during my many study sessions throughout this process.

And most of all, I would like to thank my parents, Terry and Anita, who overcame their difficult upbringings to provide a family environment from which any achievement was possible.

Contents

List of Figures

Chapter 1

Introduction

The study of human respiratory disease and pharmacological intervention has relied heavily on the use of animal models for determining exposure risk, mechanisms of disease, prevention strategies, and effects of drugs. Researchers have used a variety of methods for assessing the pulmonary response of laboratory animals to various toxins and pharmacological agents. Many of these methods are destructive or invasive in nature. For many years, researchers have been interested in developing pulmonary function tests which are noninvasive in nature and relatively simple to administer. These tests are of particular advantage for studies involving mice, where often large numbers of animals are utilized. Using tests that are simple to administer generally translates to more efficient and more accurate data collection. Noninvasive testing results in less stress placed on the animal and allows repeated measurements on the same animals at multiple time points. This reduces the number of animals needed to perform these studies and results in collection of more scientifically sound data.

Measurement of pulmonary function in conscious, unrestrained mice has traditionally been accomplished using a whole-body plethysmograph (WBP). Using this system, an animal is placed in a chamber where pressure changes due to respiration are observed, which are then related to pulmonary function. The advantages of this type of system include extreme ease of use, little stress on

the animal, and the ability for repeated and prolonged measurements.

Drorbaugh and Fenn [12] related tidal volume to the pressure changes measured in a closed chamber due to thermo-hygrometric differences between respired air and gas within the chamber. Epstein and Epstein [15] later corrected the assumption that these thermo-hygrometric effects were symmetric during inspiration and expiration. Jacky [23] and Epstein et al. [16] proposed methods to account for the theoretical considerations in Epstein and Epstein's work [15]. All these methods assume plethysmograph pressure can be accounted for solely by temperature and humidity.

It is known however, that gas compression in the lung can also contribute significantly to the pressure measured in an unrestrained plethysmograph. Hamelmann, et. al. [22] developed an empirical index call Enhanced Pause (Penh), which was said to reflect changes in airway resistance (increased airway resistance results in an increase in gas compression). Frazer, et. al. [19] demonstrated the effects of compression on the WBP signal with a model validated by simultaneously measuring plethysmograph pressure and chest wall motion of guinea pigs with a laser displacement sensor. Enhorning, et. al. [14] used a mechanical chest to show that plethysmographic pressure was not only affected by breathing pattern, but also by airway resistance. Although there is some controversy as to the extent and conditions under which gas compression becomes a significant portion of the WBP signal measured in mice [11, 27, 31, 26], it is clear that tidal volume measurements of mice with increased airway resistance or breathing rate are likely to be inaccurate. Likewise, it is perhaps impossible to separate changes in gas compression (related to specific airway resistance) from changes in respiratory pattern using a traditional WBP. In this research, a new plethysmograph is proposed that uses acoustics to make an additional measurement, allowing separation of the tidal volume signal from the gas compression component.

The thesis of this research was that a traditional whole-body plethysmograph could be redesigned as a resonating cavity such that changes in mouse size, due to respiration, would sufficiently modulate the amplitude of a fixed fre-

quency excitation to provide a measurement of thoracic breathing pattern as well as the traditional plethysmograph flow signal. The additional measurement is critical for permitting estimation of lung mechanical parameters. In a traditional WBP, the pressure drop across a resistive element is utilized to measure flow. In this case, higher resistance makes for a more sensitive flow measurement. However, a higher resistance in a resonating system produces a less sharp (i.e. flatter) resonant curve which reduces the sensitivity of the acoustic modulation. So, designing a resonating cavity WBP, or acoustic whole-body plethysmograph (AWBP), is a trade-off between sensitivity of plethysmograph flow measurement and sensitivity of mouse volume change measurement.

The objective of the first phase of this research was to determine if it was possible to design a resonator with enough sensitivity for mouse volume measurement even without the presence of a flow pneumotach (i.e. very low resistance). In a traditional WBP, a typical chamber volume is approximately $350\ mL$. Since, a typical mouse tidal volume is on the order of $200\ \mu L$, the volume modulation caused by respiration of the mouse is very small. Therefore, in order for the amplitude modulation of the acoustic resonator to be perceptible, the resonator must be very highly tuned. In this phase of the research, it was demonstrated that such a chamber could be designed to be an effective plethysmograph.

The results of the first phase of this research were achieved by sacrificing the traditional plethysmograph flow measurement by minimizing the flow resistance of the nozzle. In phase two of this research, the objective was to develop a system capable of measuring both mouse volume change and plethysmograph flow. This objective was achieved and the utility of the system was demonstrated by using the measurements to estimate specific airway resistance in mice challenged with a bronchoconstrictive agent.

Chapter 2

Background

2.1 Modeling physical systems with electric circuit analogues

The equations describing mechanical and fluid flow systems can be written in identical form to those describing electric circuit systems. Since circuit analysis tools and techniques are well developed, it is convenient to model physical systems using electric circuit analogues. This practice is widely used in the literature and will be used extensively in this research.

Pressure and volume flow in fluid systems are analogous to voltage and current, respectively, in electrical systems. With these analogies it is easy to show that flow resistance is represented by a resistor, gas compliance is represented by a capacitor, and gas inertance is represented by an inductor. Using these relations, electric circuit models can be developed which will be used for analysis of small animal plethysmography.

2.2 Modeling the respiratory system

In order to describe some of the measurements made using the unrestrained, or whole-body plethysmograph, an understanding of the traditional models of the respiratory system is warranted. A simple "black box" model of the respiratory system is shown in Figure 2.1. A pressure at the body surface, $P_{bs}(t)$,

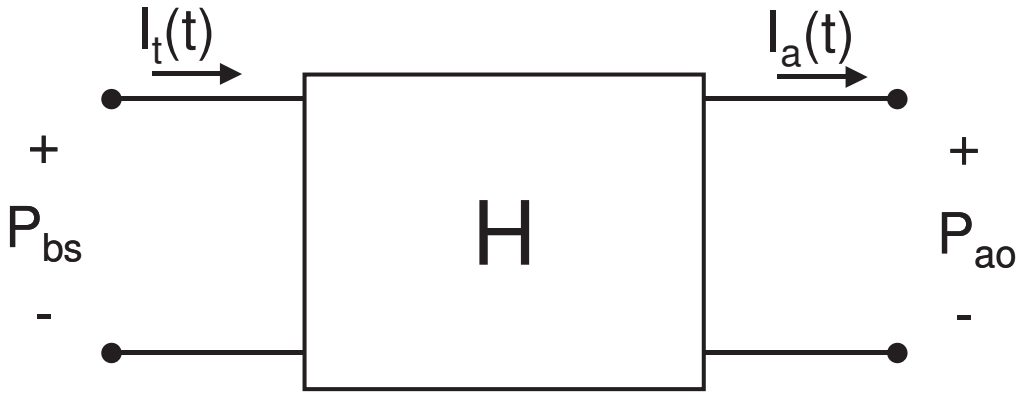

Figure 2.1: Simple input-output model of respiration where $I_t(t)$ represents flow produced by movement of the thorax, $P_{bs}(t)$ is pressure at the body surface, H represents the mechanical properties of the respiratory system, $I_a(t)$ is the flow out of the airways of the animal, and $P_{ao}(t)$ is pressure at the airway opening.

produces a flow of gas, $I_t(t)$, that is forced through the respiratory system, H. As this flow moves through the system it is filtered by the mechanical properties of H, resulting in a flow, $I_a(t)$, and a pressure, $P_{ao}(t)$, at the airway opening.

A common representation of H is the six-parameter Dubois respiratory model [13] shown in Figure 2.2. In this model, P_{alv} is the alveolar pressure, R_{aw} is the airway resistance, L_{aw} is the airway inertance, and C_g accounts for gas compressibility in the alveolar space. Similarly, the chest wall and muscle tissue impedance are represented by R_{ti}, L_{ti}, and C_{ti}.

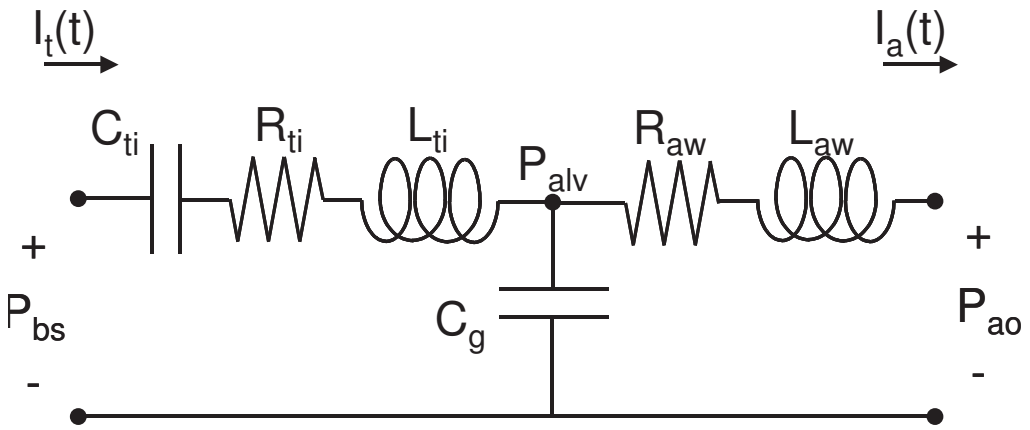

Figure 2.2: Dubois respiratory model.

With a freely respiring animal, the current $I_t(t)$ is produced by movement of the thoracic muscles. Since this current is independent of the tissue impedance, the tissue elements can be neglected. Additionally, at normal breathing frequencies, the impedance of the inductor L_{aw} is also negligible (see, for example, [21]). Thus, for a freely respiring animal, we are left with the simple circuit shown in Figure 2.3. In this model, $I_a(t)$ is flow at the airway opening and is assumed to be measured at near alveolar conditions.

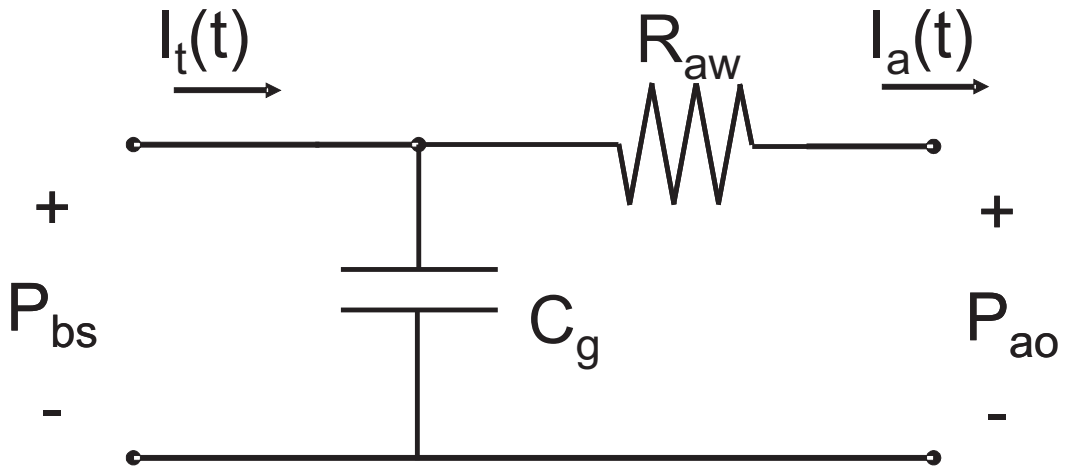

Figure 2.3: Simple RC respiratory model.

As the warmed humidified gas exits the respiratory system, it cools as it mixes with the ambient air. There is evidence that this cooling process has a significant time constant associated with it (i.e. it is not instantaneous) in humans [35, 34]. Tests in our laboratory indicate that this effect is nearly instantaneous in rats, and presumably in smaller animals such as the mouse. On inspiration, the reverse takes place. That is, the ambient gas expands as it is warmed and humidified. When the thermal effect is instantaneous, it is simply acts as a gain, G, on the airway flow. The value of G [34] is:

$$G = 1 - \frac{T_i}{T_a} \cdot \left[\frac{P_B - P_{H2Oa}}{P_B - P_{H2Oi}} \right] \tag{2.1}$$

where the subscripts i and a denote conditions of inspired and alveolar gas, respectively, and T and P are temperature and pressure, respectively.

If we let $\tau = \frac{1}{RC}$ and transform to the Laplace domain, the resulting model is shown in Figure 2.4 where $I_y(t)$ is flow measured after cooling on expiration and before heating on inspiration.

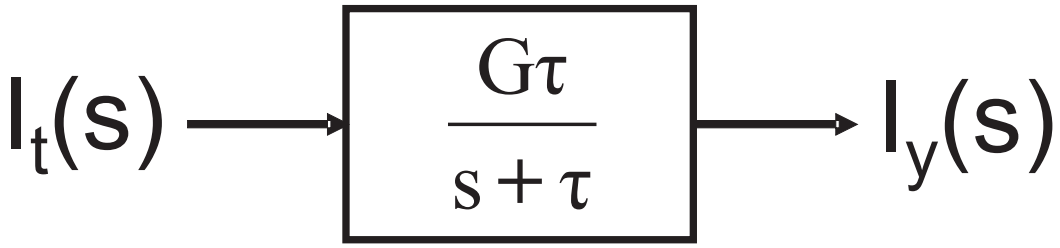

Figure 2.4: Laplace input-output model of respiratory system.

2.3 Specific airway resistance

A common measurement seen in the literature has been termed "specific airway resistance". Typically, this measurement is derived from $I_a(t)$ and $I_t(t)$ shown in Figure 2.3 and measured using a double chamber plethysmograph. The double chamber plethysmograph restrains the animal and places a seal around the neck in order to independently measure the required flows. Specific airway resistance is defined as:

$$S_{Raw} \equiv R_{aw} \cdot TGV \tag{2.2}$$

where TGV is thoracic gas volume. Gas compliance in the lung is:

$$C_g \equiv \frac{TGV}{P_B} \tag{2.3}$$

By substitution of Equation 2.3 into Equation 2.2, it is seen that specific airway resistance is nothing more than the time constant RC multiplied by barometric pressure P_B:

$$S_{Raw} \equiv R_{aw} \cdot C_g \cdot P_B \tag{2.4}$$

While it is true that this multiplication removes a known parameter from the measurement, it seems more intuitive from an engineering perspective to simply measure (or estimate) the time constant. Therefore, when specific airway resistance is referred to in this research, it is generally referring to RC.

2.4 Whole Body Plethysmograph

The whole-body plethysmograph (WBP) is simply a chamber in which an animals is placed where it is free to move around and breath spontaneously. Typically, flow into and out of the chamber is measured using a screen pneumotach as the animal respires. When an animal is placed in the WBP, there is no seal to separate the thoracic and nasal flow. On inspiration, the thorax expands creating a positive pressure. Gas is drawn into the respiratory system creating a negative pressure. The model of an animal in the WBP is shown in Figure 2.5. The reduced-form model is shown in Figure 2.6 where the plethysmograph is

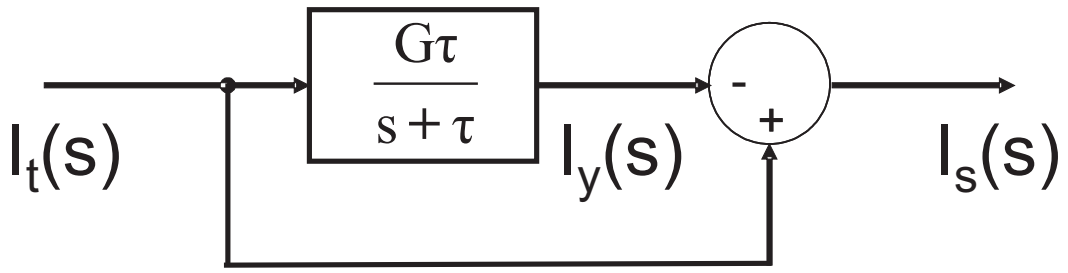

Figure 2.5: Model of the whole-body plethysmograph.

represented by a dashed line. Note that we have only a single measurement (box flow) in this system.

2.4.1 Tidal Volume

In the setup above it is not possible to determine the transfer impedance of the lung since the input (the thoracic flow) is unknown. Likewise, it is not possible to determine the thoracic flow since the transfer impedance is unknown. When used to measure tidal volume, the assumption is that there is no gas compression. When there is no gas compression, then $\tau \rightarrow \infty$, and the model reduces

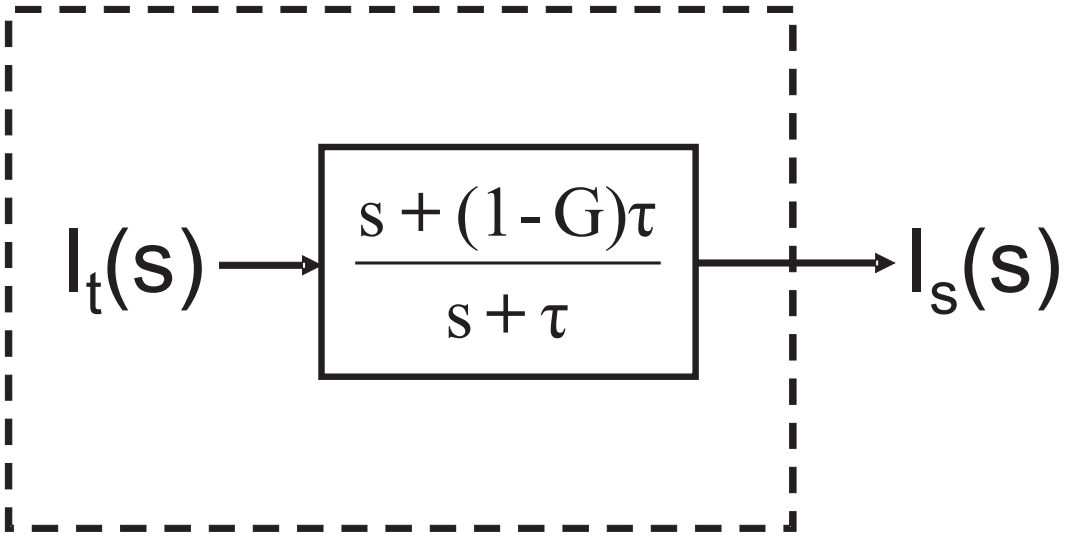

Figure 2.6: Reduced form model of the WBP.

to a gain as shown in Figure 2.7. Since the gain is known, the tidal volume can be calculated:

$$V_t(t) = \int I_t(t)dt = (1-G)\int I_s(t)dt \tag{2.5}$$

As previously mentioned, the compression factor may be extremely small in normal mice. In sick animals, or when the breathing rate is elevated, gas compression may become an important consideration and tidal volume calculated in this manner is likely inaccurate.

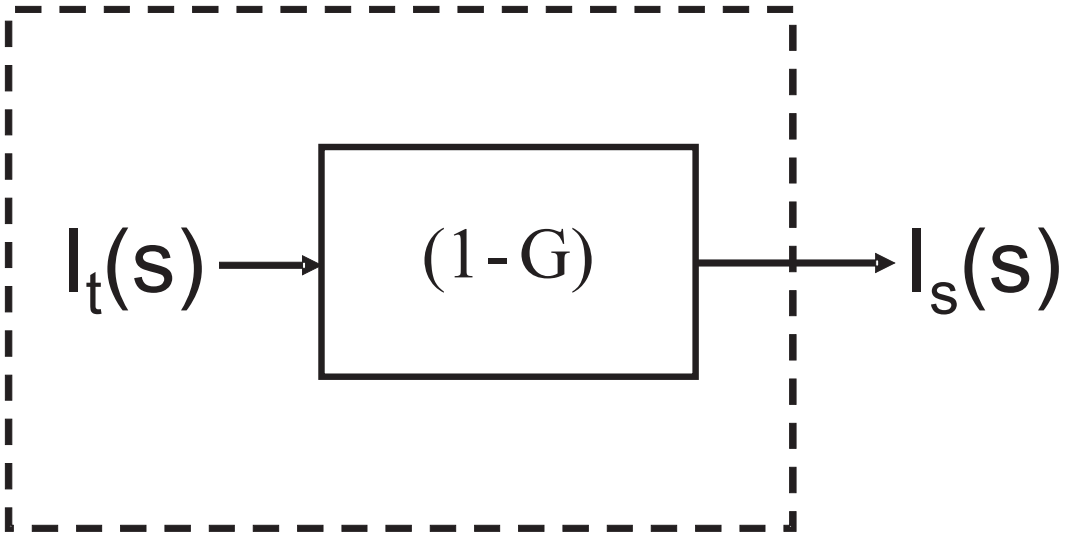

Figure 2.7: WBP model when $\tau \rightarrow \infty$.

2.4.2 Penh

A method that has often been used as a surrogate indicator of change in airway impedance is the index enhanced pause (Penh) [22]. Penh is defined as:

$$Penh = \frac{P_E}{P_I} \cdot \left[\frac{T_E}{T_R} - 1\right] \tag{2.6}$$

where P_E is peak expiratory flow, P_I is peak inspiratory flow, T_E is expiratory time, and T_R is relaxation time (Fig 2.8). Relaxation time is defined as the time it takes to reach 64 percent of total expiratory volume. Penh is an empirical index that has been suggested as an indicator of airway resistance. Although Penh may correlate well with airway resistance under some circumstances, its reliability as a primary indicator of airway reactivity has been questioned [11]. Recently, based on a theoretical and experimental analysis of unrestrained plethysmography with mice, Lundblad et. al. [27] have concluded that Penh should not be used to assess bronchial responsiveness, an opinion shared by other investigators as well [31].

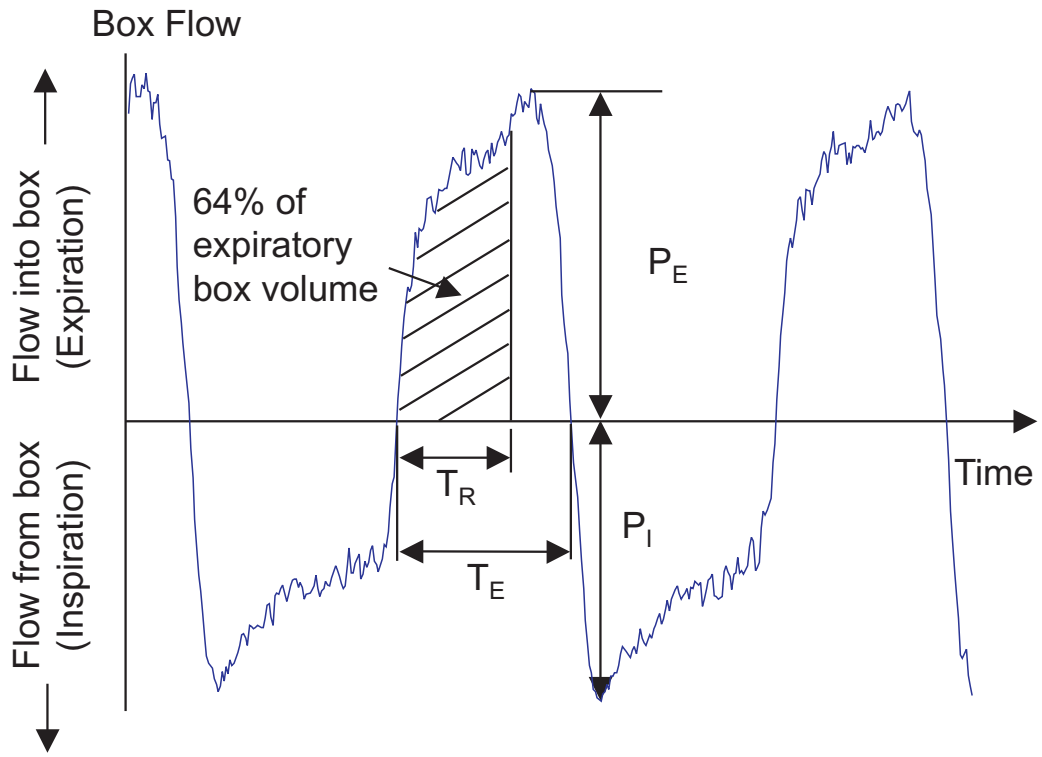

Figure 2.8: Parameters for Penh.

2.5 Helmholtz Resonator

A cavity with and open neck, or nozzle, such as the one shown in Figure 2.9 is known as a Helmholtz resonator [4]. When considering acoustic wavelengths

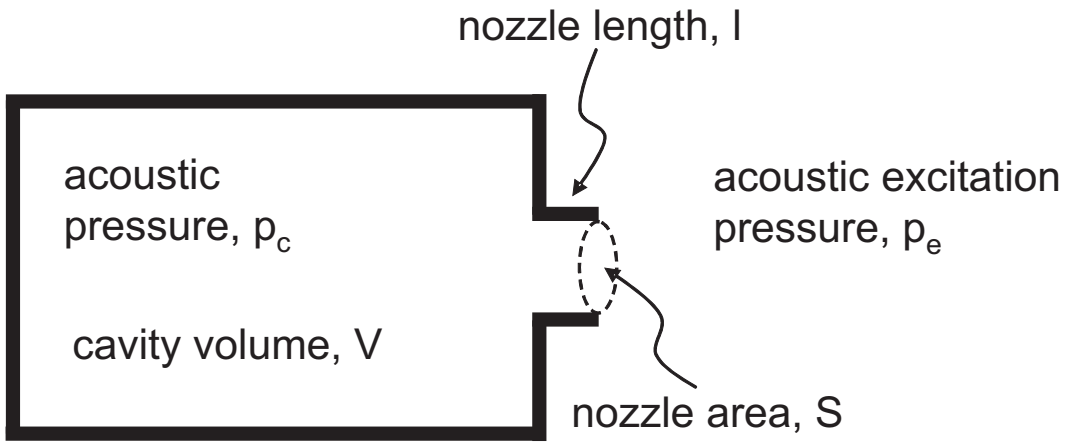

Figure 2.9: Helmholtz resonator.

much larger than cavity dimensions, a lumped parameter model is prescribed. The equivalent circuit for the such a resonator with an external excitation, p_e, is shown in Figure 2.10, where the capacitor represents the gas acoustic compliance in the cavity, the inductor represents the gas mass momentum of the plug of air in the nozzle, the resistor represents the acoustic resistance of gas in the nozzle, and p_c is the acoustic pressure in the chamber. The complex impedance of the circuit is:

$$Z(j\omega) = R + j\omega L - j\frac{1}{\omega C} \tag{2.7}$$

The current in the circuit is maximum when the reactance of the inductor and the reactance of the capacitor cancel. The frequency at which this happens is

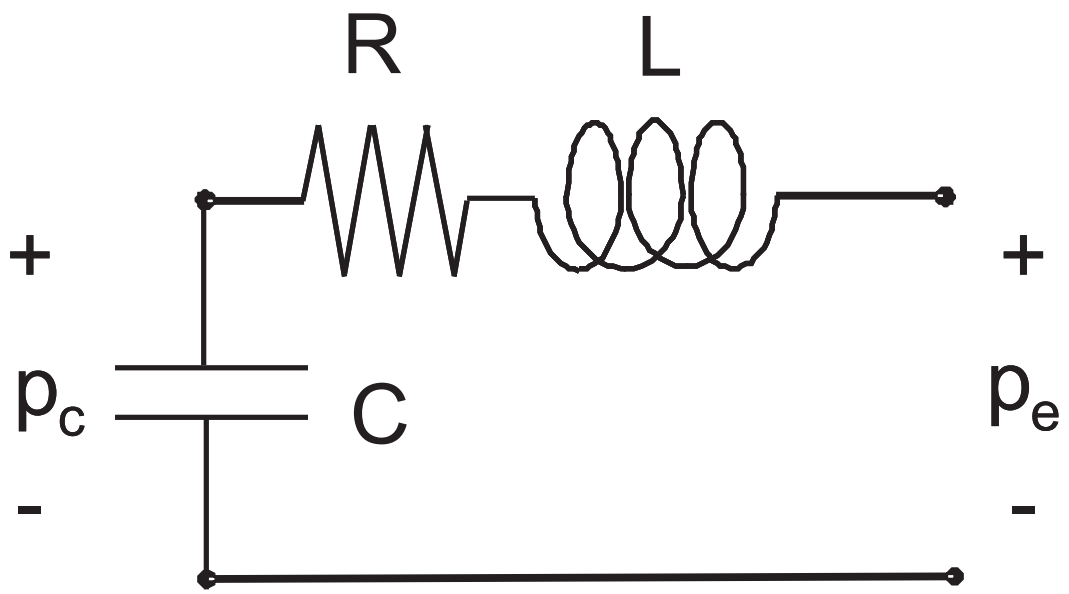

Figure 2.10: Equivalent circuit for a Helmholtz resonator with an external excitation.

called the resonant frequency, ω_o.

$$\omega_o L = \frac{1}{\omega_o C} \tag{2.8}$$

$$\omega_o^2 = \frac{1}{LC} \tag{2.9}$$

$$\omega_o = \frac{1}{\sqrt{LC}} \tag{2.10}$$

Furthermore, the current, i, in the circuit can be found from both the ratio of the excitation pressure to the circuit impedance and/or the ratio of the chamber pressure to the capacitor impedance:

$$i(j\omega) = \frac{p_e(j\omega)}{R + j\omega L + 1/j\omega C} = \frac{p_c(j\omega)}{1/j\omega C} \tag{2.11}$$

So the ratio of the chamber pressure to excitation pressure is

$$\frac{p_c(j\omega)}{p_e(j\omega)} = \frac{1}{1 - \omega^2 LC + j\omega RC} \tag{2.12}$$

Also, using Equation 2.9

$$\frac{p_c(j\omega)}{p_e(j\omega)} = \frac{1}{1 - \omega^2/\omega_o^2 + j\omega RC} \tag{2.13}$$

Finally, amplitude of the chamber acoustic pressure to the excitation acoustic pressure is:

$$\left|\frac{p_c(j\omega)}{p_e(j\omega)}\right| = \frac{1}{((1 - \omega^2/\omega_o^2)^2 + \omega^2 R^2 C^2)^{\frac{1}{2}}} \tag{2.14}$$

Chapter 3

Acoustic Plethysmograph for Tidal Volume

3.1 Materials and Methods

3.1.1 Theory

The plethysmograph operates as a resonant cavity, or Helmholtz resonator such as the one described in Section 2.5. From Equation 2.14, a sinusoidal source with amplitude p_e will produce a pressure signal amplitude inside the cavity given by:

$$p_c = \frac{p_e}{[(1-\omega^2/{\omega_o}^2)^2 + \omega^2 R^2 C^2]^{\frac{1}{2}}} \tag{3.1}$$

Both w_0 and C are dependent on the volume, V, of the cavity and can be described by the following equations [4]:

$$w_0 = \sqrt{\frac{c_0^2 S}{lV}} \tag{3.2}$$

$$C = \frac{V}{\rho_0 c_0^2} \tag{3.3}$$

In these expressions, c_0 is the speed of sound, S is the nozzle cross sectional area, l is the effective length [4] of the nozzle, and ρ_0 is the density of air. Figure 3.1 shows the magnitude of p_c/p_e versus volume for a chamber with nozzle dimensions $l = 4\ cm$, $S = .785\ cm^2$, and a resistance of $R = 0.0004$ $cmH_2O\ sec\ cm^{-3}$. The peak output occurs at approximately 77 mL. To the left of the peak, there is a region on the curve that is nearly linear. The midpoint of this region is denoted V_x on the graph, and represents the operating point of the plethysmograph. When the acoustic excitation (p_e) is held at a constant frequency and amplitude, small perturbations about V_x will produce essentially linear changes in the output acoustic pressure amplitude (p_c).

The concept of the AWBP is to place an animal in the plethysmograph and adjust the chamber volume such that the volume of air surrounding the animal (the deadspace) is V_x. As the animal respires and its chestwall expands and contracts, the deadspace volume changes which modulates the amplitude of the acoustic pressure in the chamber. Inspiration corresponds to a decrease in output amplitude while expiration corresponds to an increase in output amplitude. Based on orifice and tube impedance models (see for example [32]), the acoustic input impedance of the mouse respiratory system, beginning with the large change in area from the chamber to the nasal opening, is very large. For this reason, the volume of air inside the mouse lungs has little or no effect on the acoustic pressure in the plethysmograph.

There is a direct correlation between the signal to noise ratio of volume mea-

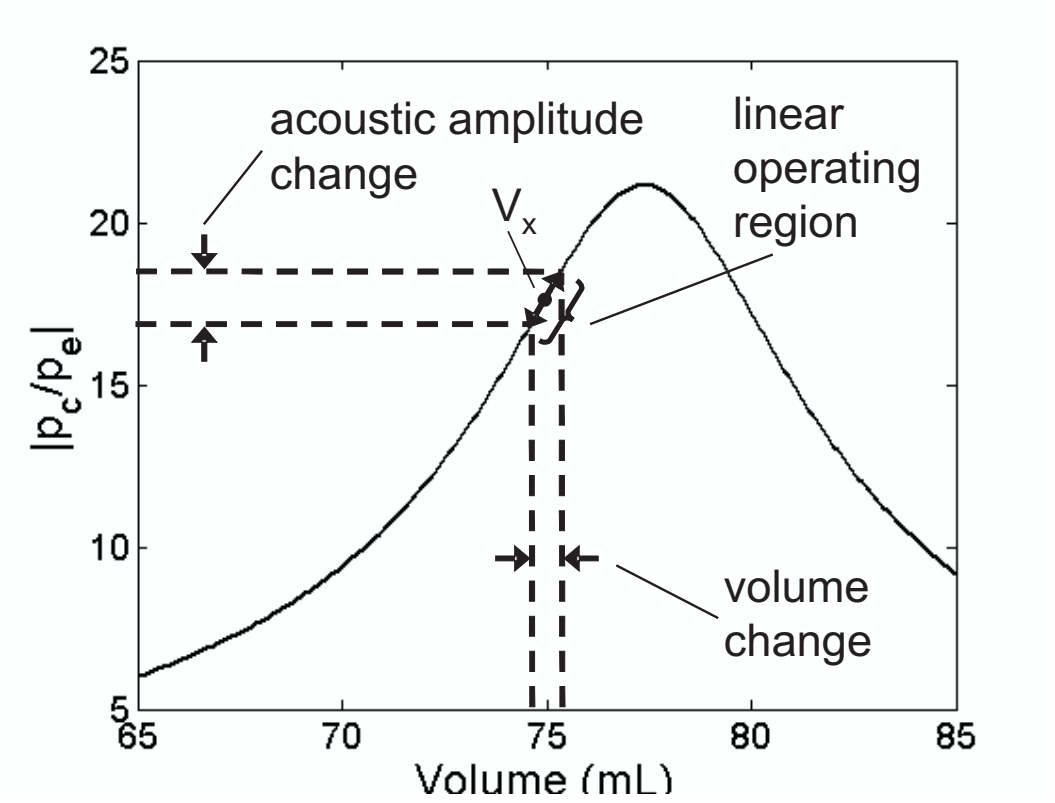

Figure 3.1: Magnitude of the excitation to chamber acoustic pressure ratio versus cavity volume. Small perturbations about the operating volume, Vx, produce linear changes in the chamber acoustic pressure amplitude.

surements and the sound pressure level (SPL) inside the chamber. For this reason, the sensitivity of the system is increased with an increased SPL. Since the excitation frequency is near 300 Hz and the hearing range of the mouse does not extend below 2000 Hz [20, 17], a higher SPL can be tolerated than has been used in systems designed for humans.

3.1.2 System

A diagram of the mouse plethysmograph used in this study is shown in Figure 3.2. A photograph of the prototype system is shown in Figure 3.3. The

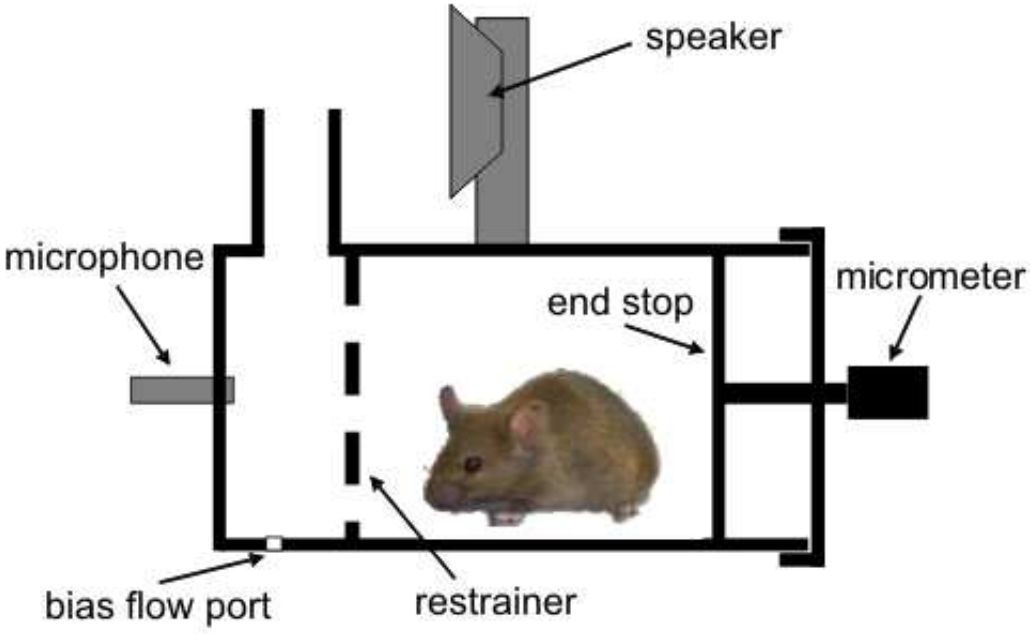

Figure 3.2: Schematic of the acoustic plethysmograph.

plethysmograph consisted of a main chamber, nozzle, speaker, and end stop assembly. The main chamber was constructed from a plexiglass tube with a 3.68 cm internal diameter. A microphone was mounted in a fixed plate which

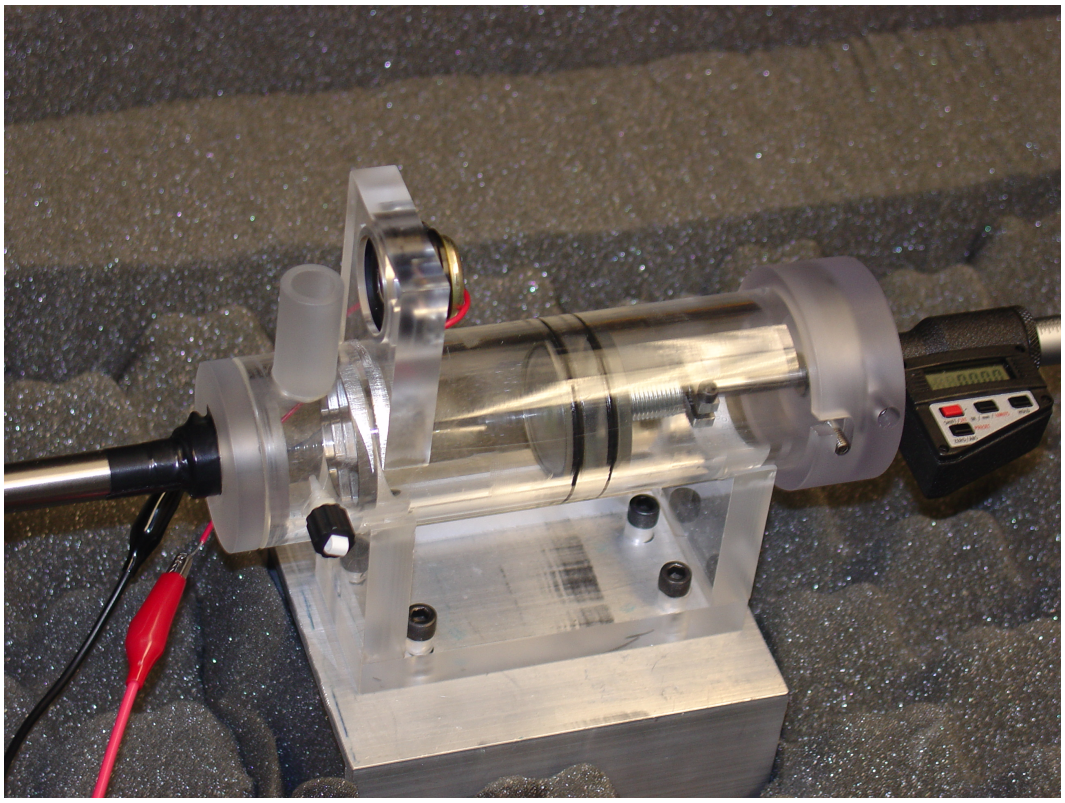

Figure 3.3: Photograph of the prototype acoustic plethysmograph.

sealed one end of the chamber. The opposite end of the chamber was sealed with an adjustable end stop that was used to set the chamber volume for each mouse. The end stop was connected to a micrometer (The L.S. Starrett Company, Model 762) through a removable end cap connected to the main chamber. The micrometer head was used to adjust the chamber volume which could be varied from approximately 60 to 120 mL.

The nozzle was 3.5 cm long with an internal diameter of 1.1 cm. The nozzle was located near the front of the main chamber between the microphone and a small stainless steel restrainer. The restrainer confined the mouse to the back of the plethysmograph such that the nozzle could not be occluded. A small port in the chamber could be used to introduce a bias flow of air to flush out carbon dioxide and keep the animal cool. The impedance of this port and associated tubing must be large so as not to affect the resonance of the system (see for example [32]).

The speaker was driven by a function generator (Medi Cal Instruments, Inc., Model 220) with a sine wave output. Acoustic pressure inside the chamber was measured with a Larson Davis microphone (Model 2530 microphone, Model 910B pre-amp, Model 2200C power supply). Since the plethysmograph was tested in a very noisy laboratory environment, the system was shielded by placing it in a box lined with acoustic foam. All data were digitized at a rate of 10 kHz with a 16-bit data acquisition board and custom program (National Instruments, Model 6063E and LabView) after passing through a 1 kHz anti-aliasing filter (National Instruments, Model SC-2345 and SCC-LP04).

3.1.3 Signal Processing

The signal processing in this application was performed using Matlab (The Mathworks). The system is designed to be excited by a single frequency (f_o) constant amplitude sine wave. The acoustic pressure signal measured inside the chamber was first passed through a band pass filter with corner frequencies

at $f_o - 15\ Hz$ and $f_o + 15\ Hz$. The amplitude was demodulated by calculating the magnitude of the Hilbert transform [28]. This voltage was then related to tidal volume using the calibration described below.

3.1.4 Calibration

The excitation frequency of the system was selected by setting the chamber volume to 75 mL. The frequency of the function generator was adjusted in the 250 to 350 Hz range until the maximum output signal was obtained. Next, a mouse was placed in the chamber, which decreased the plethysmograph dead space. Note that the output signal varied as the animal's volume changed during respiration. The DC component of this signal represents the output at the average dead space volume. The plethysmograph volume was adjusted until the DC output was maximized. This represents the peak output amplitude at this excitation frequency and chamber dead space volume. The plethysmograph volume was then decreased by 2 mL in order to move from the peak of the output curve to the linear operating region (i.e. V_x in Figure 3.1). This designates the operating point of the plethysmograph. The excitation amplitude was next adjusted until the mean SPL in the chamber was 110 dB. A three point calibration was obtained by measuring the DC voltage output at three volumes: at the operating point, at the operating point minus 400 μL, and at the operating point plus 400 μL. These calibration volumes were achieved by adjusting the digital caliper on the end stop assembly. The slope of the best straight line fit of the calibration data is the ratio of voltage to volume.

3.1.5 Testing

The accuracy of the plethysmograph system was tested by measuring the change in volume of a water-filled balloon inside the chamber connected to an external syringe pump. A 250 μL syringe was incorporated in the pump

and connected to the balloon through the plethysmograph bias flow port. The initial balloon volume was approximately 20 mL, representing the volume of a mouse. All connections were made with stiff-walled Teflon tubing. A three way valve was connected inline for initial filling of the balloon and purging of air from the system. A linear potentiometer attached to the syringe pump was used to record syringe displacement. The system was calibrated as described above. The syringe pump was programmed to move between 0 and 250 μL at 527 $\mu L/min$ (maximum speed). Because the syringe pump produced a slight vibration, the data for this test were post-processed with a 30 $msec$ moving average filter.

A step test was used to assess the response time of the system. Since the syringe pump was not fast enough for this purpose, the test was administered manually. The syringe assembly was disengaged from the screw drive and the test was performed by manually pushing the syringe assembly as fast as possible.

Finally, the plethysmograph was used to measure the tidal volume of a 19 $gram$ specific pathogen-free female A/J mouse (Jackson Laboratory). The animal was housed in an AAALAC-accredited animal facility at 23 $\deg C$ and 50 $\%$ humidity with a 12 hour light/dark cycle, and was provided standard laboratory mouse chow and tap water *ad libitum*. The mouse was weighed and placed in the chamber, and tidal volume measured.

3.2 Results

Results of the water-filled balloon test are shown in Figures 3.4 and 3.5. Note that the time scale for this test is in minutes. This was due to the speed limitations of the syringe pump. Since it is difficult to see the syringe volume signal in Figure 3.4, a zoomed view is shown in Figure 3.5. The root-mean-square error over the five minute test was 4.43 μL. The standard deviation of the error was

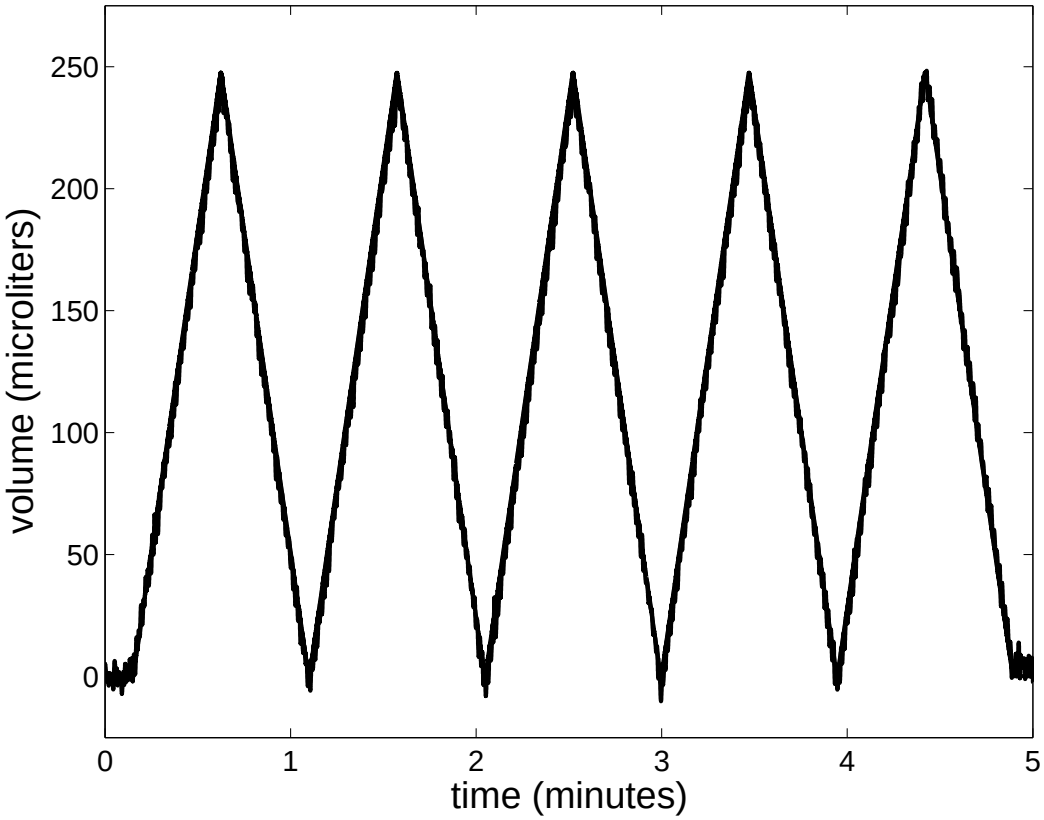

Figure 3.4: Accuracy test: syringe pump volume and plethysmograph output volume versus time.

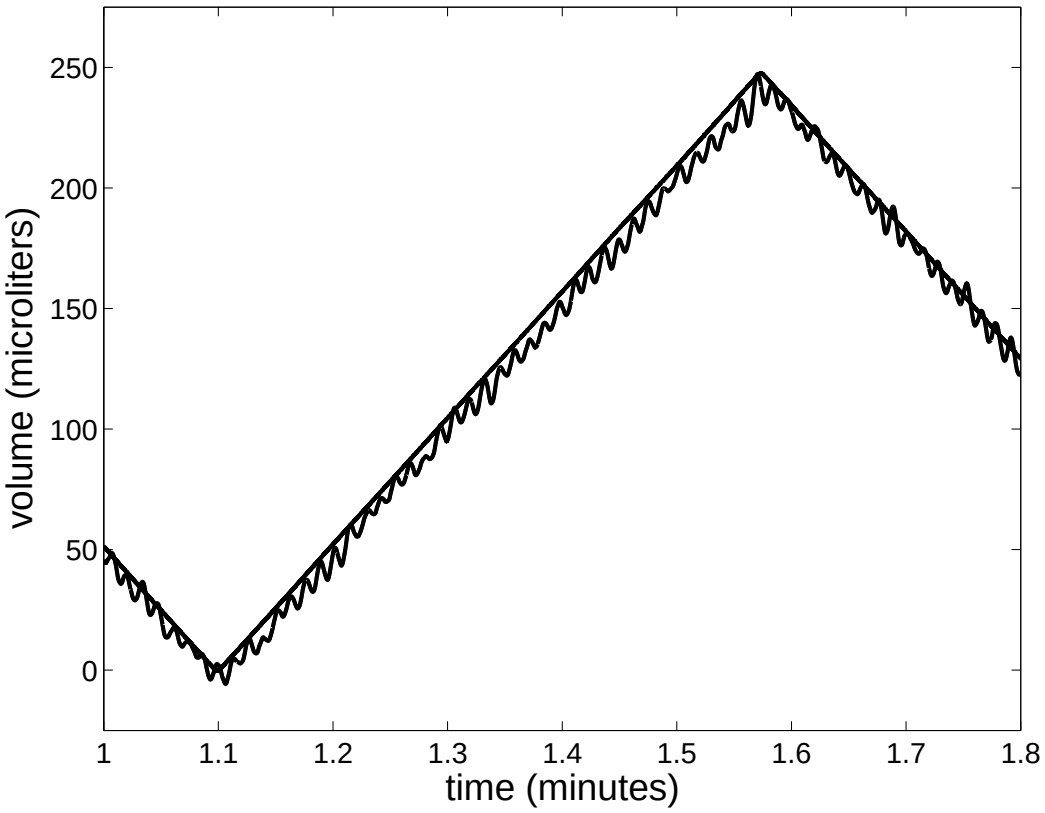

Figure 3.5: Zoomed view of syringe pump volume (smooth line) and plethysmograph output volume (noisy line) versus time.

4.09 μL.

The step test is shown in Figure 3.6. Note that since the syringe step is gen-

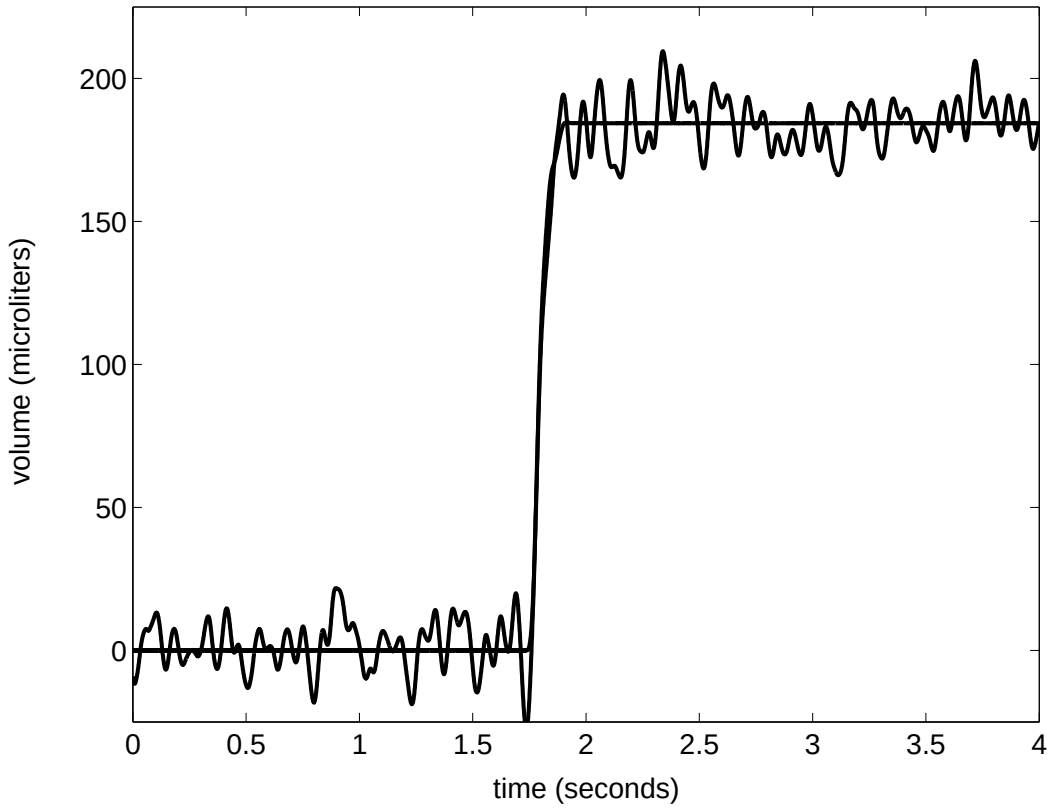

Figure 3.6: Response time test: syringe pump volume (smooth line) and plethysmograph output volume (noisy line) versus time.

erated manually, the final volume of the step is less than 250 μL. This was to avoid the noise generated by banging the end of the syringe. Also, the displacement of the syringe is not a true step. However, the results of this test demonstrate that the plethysmograph is able to track extremely fast changes in volume. The time for the input to go from 10% to 90% of the peak value was 7.91 $msec$. The 10% to 90% rise time of the output was 8.83 $msec$ giving a difference of less than 1 $msec$.

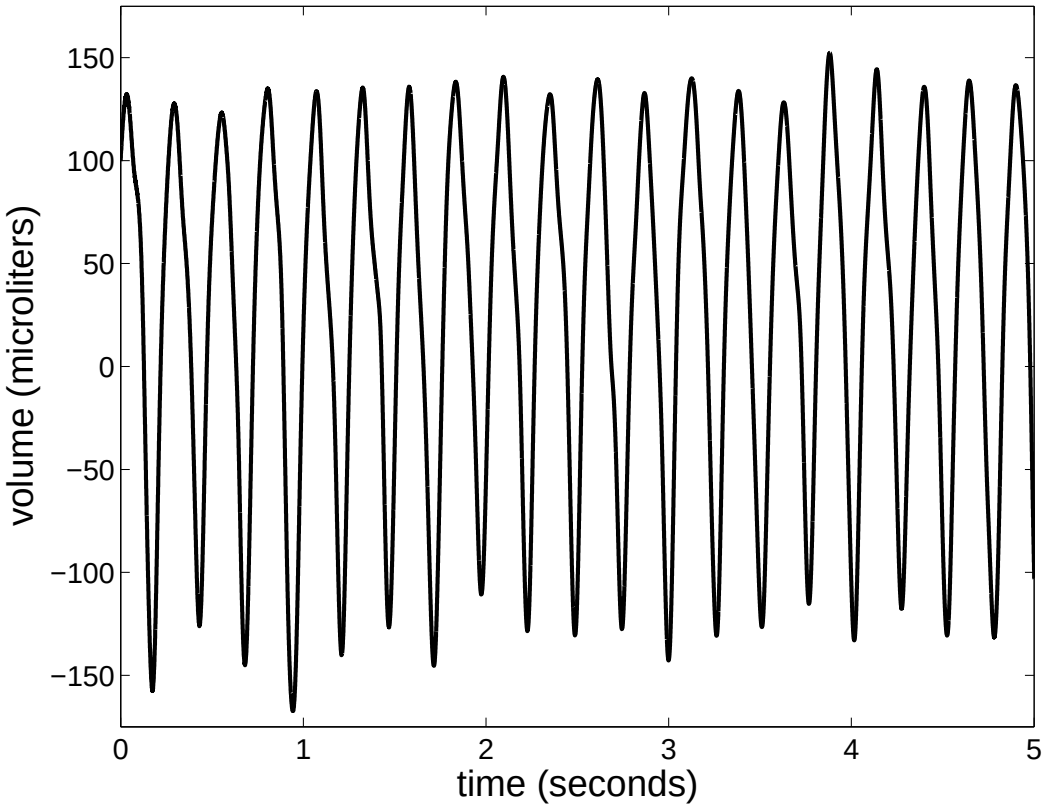

Figure 3.7: Tidal volume of an A/J mouse.

Figure 3.7 displays the plethysmograph output for the A/J mouse. The average peak-to-peak tidal volume of each breath ($\pm$ standard deviation) was 270 μL ($\pm$ 15.8 μL). The average rate of breathing ($\pm$ standard deviation) was 3.95 Hz ($\pm$ 0.196 Hz).

Chapter 4

Acoustic Plethysmograph for Specific Airway Resistance

4.1 Materials and Methods

4.1.1 System

This system is a modification of the previously described plethysmograph [36] which uses acoustics to measure the thoracic breathing pattern. Briefly, the plethysmograph operates as a resonating cavity. The amplitude of the acoustic pressure inside the cavity is determined by the cavity geometry. The volume of air surrounding a respiring mouse changes by the change in size of the mouse as it breathes. When the system is excited near the resonant frequency, the acoustic pressure amplitude in the plethysmograph is modulated in direct proportion to the change in volume of the mouse.

In the previous system [36], a low resistance nozzle was used to maximize the sensitivity of the system to changes in mouse volume. In that system, the nozzle resistance was too low to use as a pneumotachograph to measure the traditional WBP box flow. The current implementation is shown in Figure 4.1. The speaker produces a constant frequency (~ 300 Hz) acoustic signal. The micrometer is used to adjust the volume surrounding the mouse so that the chamber is in a near resonant condition, and changes in mouse volume produce linear changes in the acoustic pressure amplitude (see [36]). A screen placed across the outside end of the plethysmograph nozzle acts as a pneumotachograph to enable measurement of box flow. The pressure drop across the screen was measured with a differential pressure transducer (Setra Systems, Inc., Model 239). So the modified plethysmograph provides two measurements. A signal proportional to change in mouse volume is measured with a microphone from the high frequency (relative to breathing frequency) low-amplitude (acoustic) pressure changes. The traditional WBP signal is measured from the low-frequency change in plethysmograph pressure which is proportional to box flow. The restrainer keeps the mouse from occluding the nozzle which would affect both measurements.

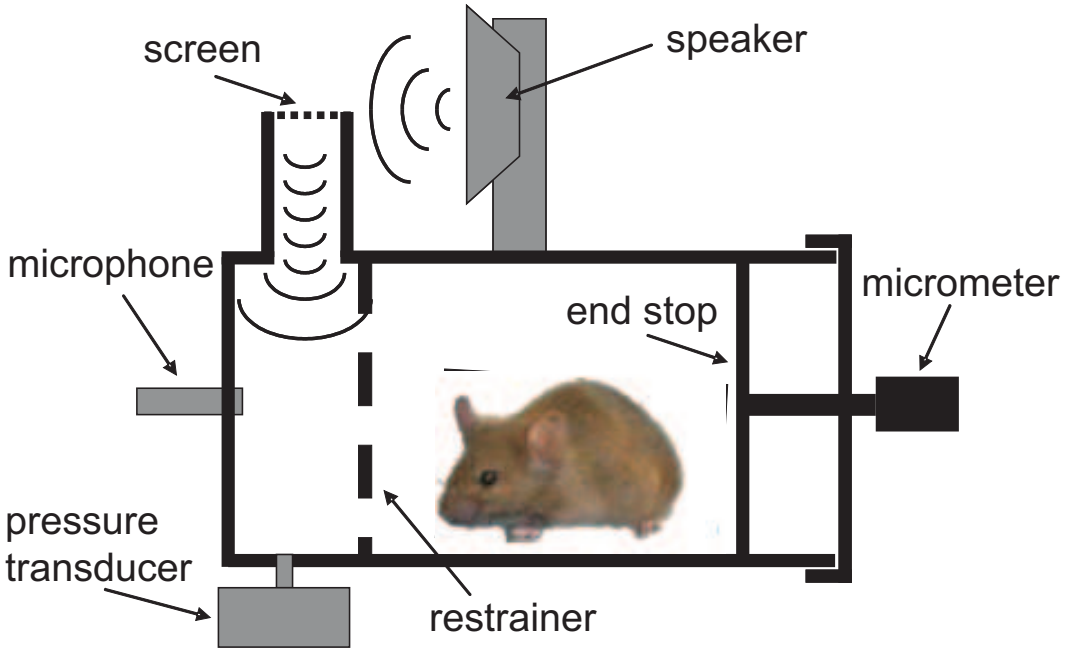

Figure 4.1: Schematic of the modified acoustic plethysmograph. The speaker generates a constant frequency ($\sim 300\ Hz$) that resonates the air in the chamber. The micrometer is used to adjust the chamber volume. Movement of the animal chest wall modulates the sound amplitude which is measured by the microphone. The pressure transducer measures the pressure drop across the screen which is proportional to flow into and out of the chamber. The restrainer inhibits the animal from occluding the nozzle.

Although the acoustic plethysmograph is designed to be a second-order system having a resonant frequency near $300\ Hz$, Sinnett, et al. [40] show that these types of flow plethysmographs act as first-order systems at low frequencies. Furthermore, they show that a flow plethysmograph with a first-order time constant of $1.5\ msec$ or less has a fast enough response for accurate measurement of forced vital capacity maneuvers in mice. Given the AWBP volume ($\sim 75\ mL$) and screen resistance ($0.00224\ \ cm\,H_2O \cdot sec \cdot mL^{-1}$), the first-order time constant is approximately $0.168\ msec$ in isothermal conditions and $0.120\ msec$ in adiabatic conditions. Since we are inferring flow from pressure at low frequencies (mouse breathing frequencies ($< 10\ Hz$)), whether the system operates in either an adiabatic or isothermal mode (or changes between the two) has little effect on the box flow measurement.

4.1.2 Model

Specific airway resistance is derived from a model [33] of the respiratory system as shown in Figure 4.2. The current source, I_t, represents the thoracic flow produced by the animal. Z_t represents the impedance of the lung tissues, I_a represents flow in the airways, R_a represents the flow resistance of the airways, and C_g represents the compressibility of the gas in the lung and airways. P_t and P_{ao} represent the pressures (relative to atmospheric pressure) produced at the thorax and airway opening, respectively. P_{alv} is alveolar pressure and P_{atm} is atmospheric pressure. Note that the direction of the currents indicated in Figure 4.2 are for expiration and are reversed during inspiration.

When an animal respires air at room conditions the gas is warmed and humidified on inspiration and the reverse (approximately) takes place on expiration. Therefore, there is an effective change in volume flow due to this thermo-hygrometric effect. This thermo-hygrometric "flow" (I_{th}) is in phase with I_a and

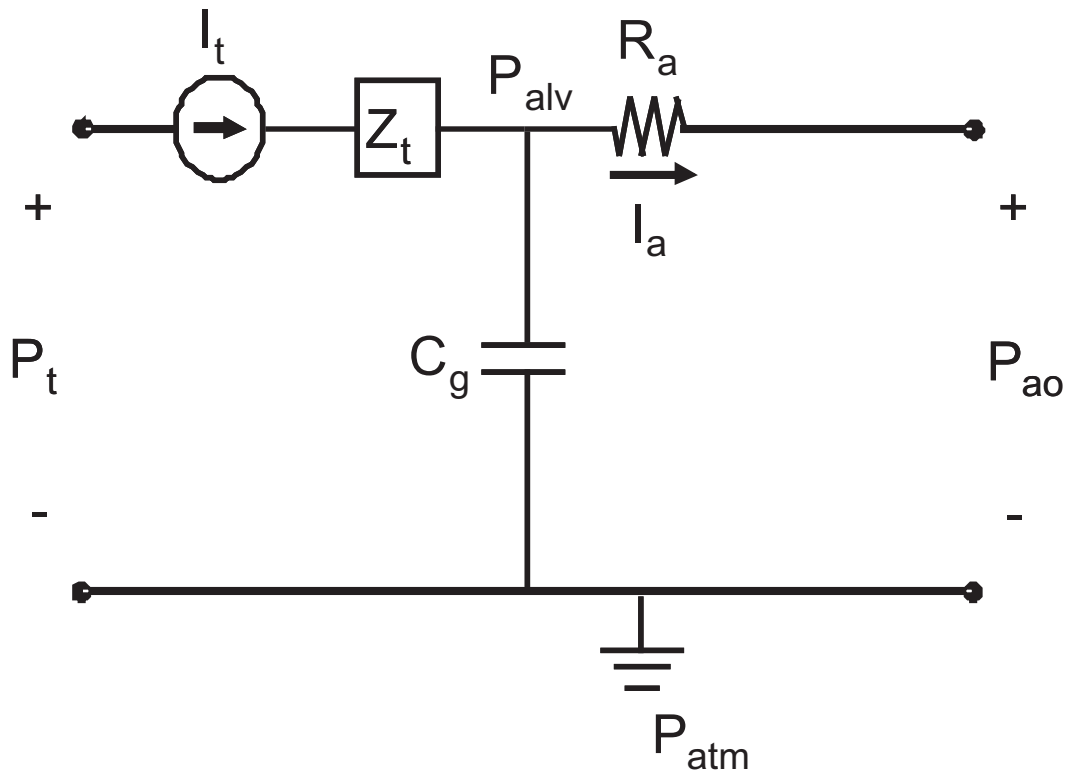

Figure 4.2: Simple model of the respiratory system [33]. I_t represents flow produced by the thorax, Z_t represents tissue impedance, R_a is airway resistance, and C_g represents compliance of alveolar gas. P_t represents pressure produced at the thorax and P_{ao} is pressure at the airway opening. P_{alv} and P_{atm} represent alveolar and atmospheric pressure, respectively.

can be modeled as:

$$I_{th} = GI_a \tag{4.1}$$

where G is [12] given by:

$$G = \left[1 - \frac{T_c(P_a - P_{H_2Oa})}{T_a(P_c - P_{H_2Oc})}\right] \tag{4.2}$$

where the subscripts c and a denote conditions of chamber and alveolar gas, respectively, and T and P are absolute temperature and pressure, respectively. Incorporating this effect results in the model shown in Figure 4.3.

It has been suggested that differences between inspiratory and expiratory conditions would necessitate separate calculations of G [15, 31, 29]. Consider an animal placed inside a whole-body plethysmograph. During inspiration, the gas is warmed from chamber temperature to body temperature and humidified from chamber humidity to saturation. In man, expiratory gas exits at nasal conditions of approximately $32°C$ and saturated with water vapor [15]. While the human respiratory tract is not a very efficient heat exchanger, that of the small rodent is much more efficient. Schmid [5] studied the exit temperature of respired air for many small mammals, including several species of mouse, and found that the exit temperature to be approximately $1°C$ above ambient.

Consider a mouse inspiring air at 50% relative humidity and $22°C$, with expiratory conditions of 100% relative humidity and $23°C$. For this case, the inspiratory value of G is 0.0956 and the expiratory value is 0.0816, a difference of approximately 17%. For an animal placed in a chamber with an open nozzle, the relative humidity in the chamber will increase with each breath until the moisture added per breath is equal to the moisture leaving the chamber via diffusion. Therefore, the inspiratory G will move toward the expiratory G the longer the

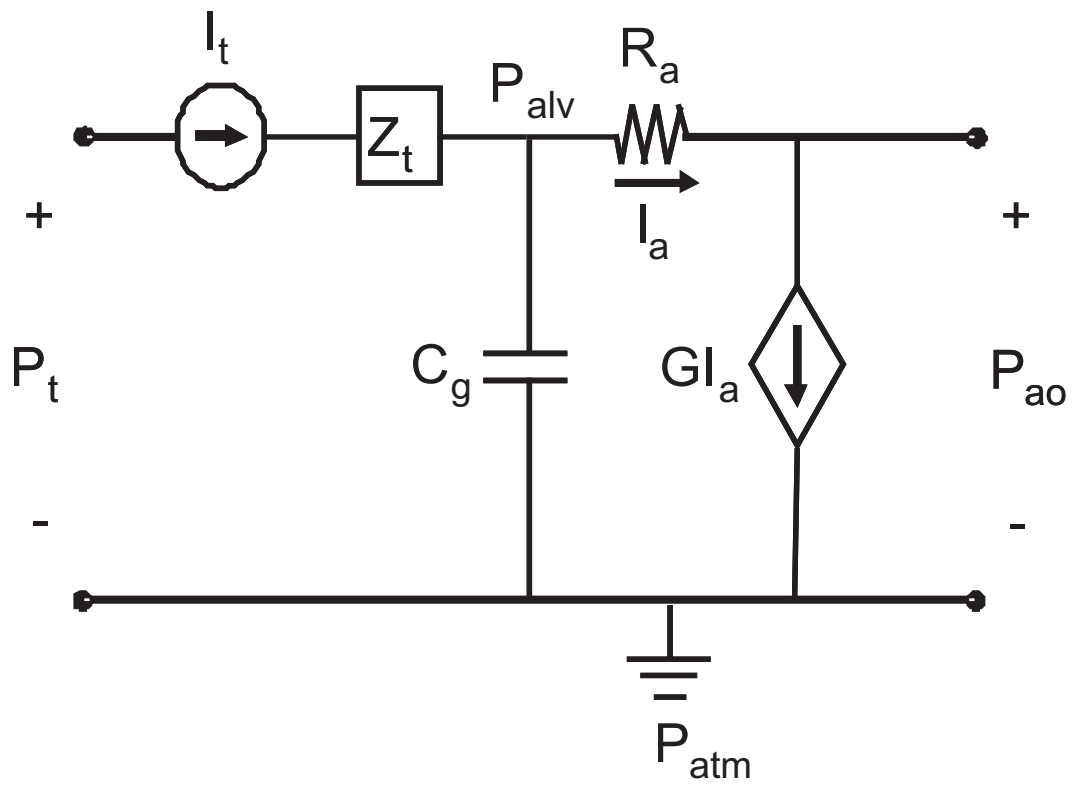

Figure 4.3: The term GI_a represents the flow "lost" on expiration ("gained" on inspiration) due to changes in temperature and humidity.

animal stays in the chamber. So there is a slight variation in G from inspiration to expiration during tidal breathing. Also, small baseline changes in G might occur if the efficiency of heating and cooling is affected by changes in respiratory rate, depth of breathing, core temperature, etc. The model used in this research considers a fixed G estimated as the average of the inspiratory G calculated at room conditions and the expiratory G calculated at 100% relative humidity and $1°C$ above room temperature. Room temperature and relative humidity during this research were $22.7°C$ and 47%, respectively. Using an assumed body temperature of $37°C$ resulted in an average G of 0.084.

Now consider an animal placed in a double-chamber plethysmograph (DCP) which is the traditional system used to estimate sRaw. This system uses a neck seal to enable simultaneous measurement of nasal flow and thoracic flow. Figure 4.4 shows the electric analogue corresponding to the DCP. Here, Z_{bc} represents the impedance of the body chamber and Z_{hc} represents the impedance of the head chamber. This system restrains the animal, but allows independent measurements of two flows (or pressures) from which sRaw can be estimated.

When an animal is placed in an unrestrained whole-body plethysmograph (WBP), there is an interaction between the thorax and nasal flows (i.e. no neck seal). Figure 4.5 shows the electric circuit analogue corresponding to the WBP. Here, Z_b represents the box impedance.Without modification, this circuit can be redrawn as shown in Figure 4.6. This represents the low-frequency bulk flow model of the WBP.

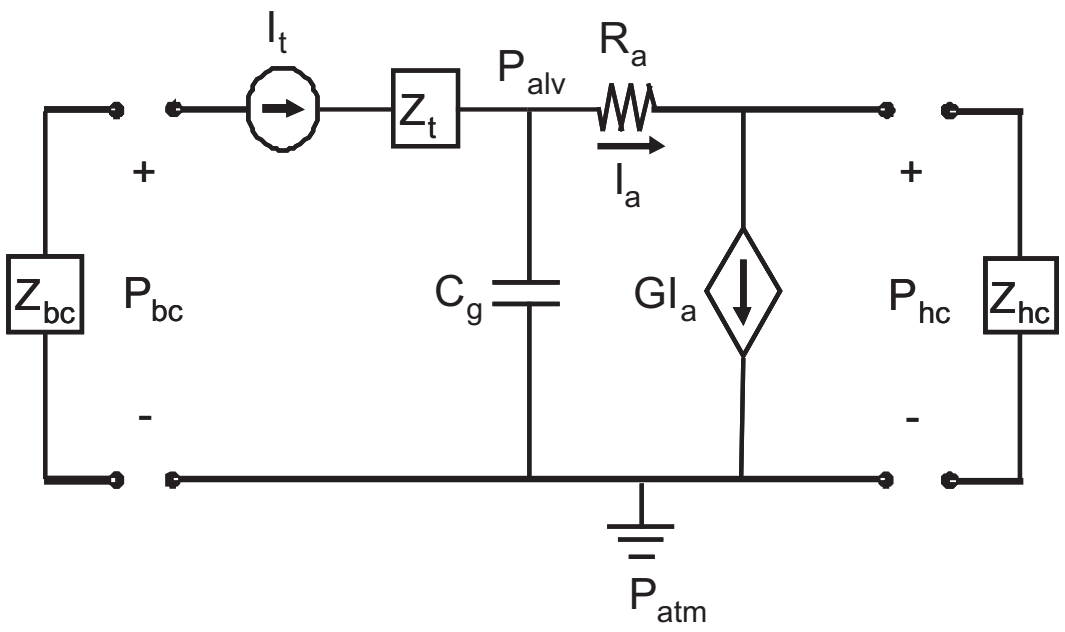

Figure 4.4: Model of the animal placed in a restrained, or double-chamber, plethysmograph. Z_{bc} and Z_{hc} represent the flow impedances of the body chamber and head chamber, respectively. P_{bc} and P_{hc} are the pressures measured in the body chamber and head chamber, respectively.

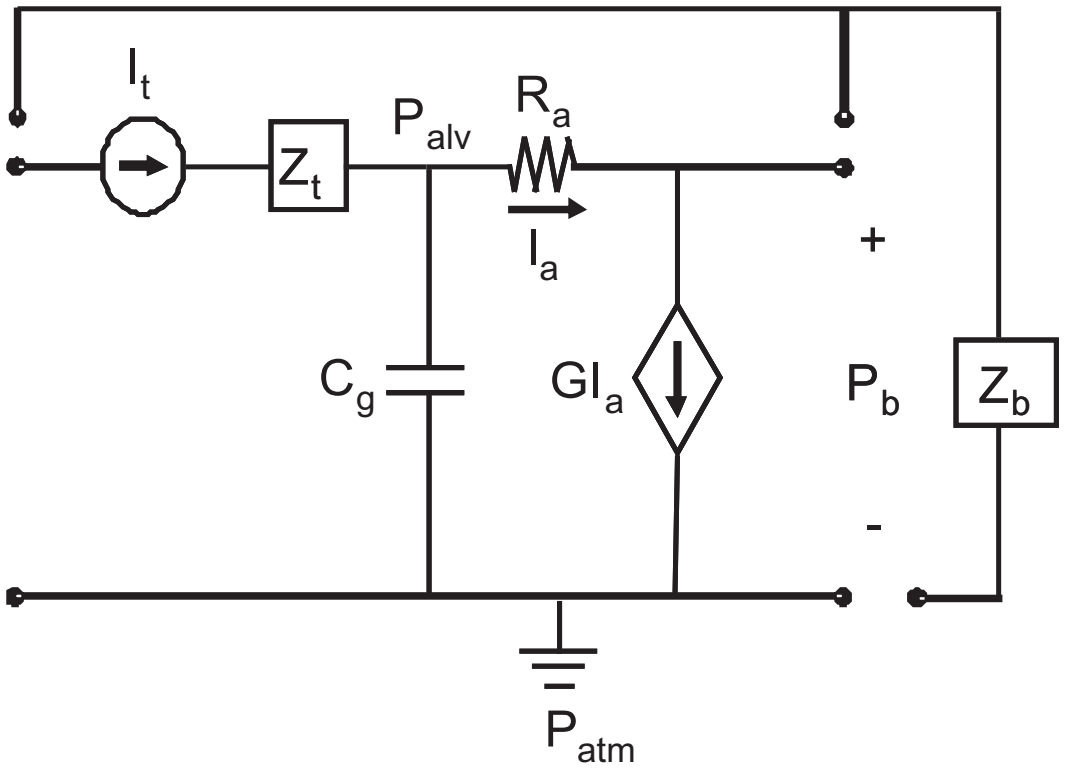

Figure 4.5: Model of the animal placed in an unrestrained, or whole-body plethysmograph. Z_b represents the box flow impedance and P_b represents the box pressure.

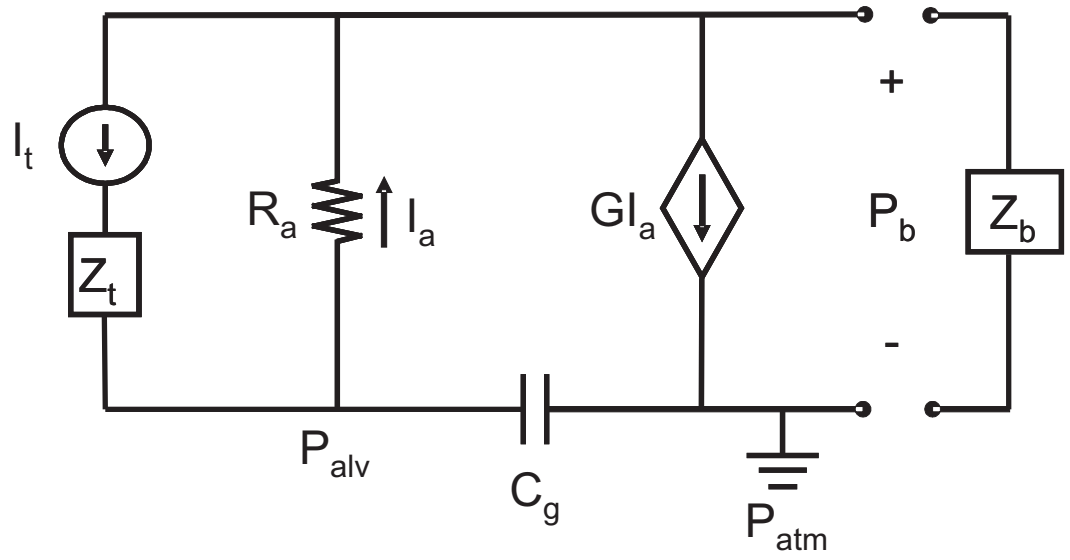

Figure 4.6: Model of animal in the unrestrained plethysmograph. This model is exactly the same circuit as in Figure 4.5. It has been redrawn in a more concise manner.

Mathematical Description

An expression for specific airway resistance can be derived based on the model shown in Figure 4.6. Summing the currents in the lung

$$I_a(t) + I_c(t) - I_t(t) = 0 \tag{4.3}$$

where $I_c(t)$ is the current into the capacitor, C_g:

$$I_c(t) = C_g \frac{dP_{alv}(t)}{dt} \tag{4.4}$$

Alveolar pressure is

$$P_{alv}(t) = R_a I_a(t) + P_b(t) \approx R_a I_a \tag{4.5}$$

Since the box pressure is extremely small compared to alveolar pressure, the box pressure term can be neglected. Substitution into the preceding equation gives

$$I_c(t) = R_a C_g \frac{dI_a(t)}{dt} \tag{4.6}$$

Now substituting this expression into Equation 4.3 and solving for thoracic flow:

$$I_t(t) = I_a(t) + R_a C_g \frac{dI_a(t)}{dt} \tag{4.7}$$

Summing the currents at the airway opening

$$I_b(t) + I_a(t) - G I_a(t) - I_t(t) = 0 \tag{4.8}$$

Solving for airway flow

$$I_a(t) = \frac{I_t(t) - I_b(t)}{1 - G} \tag{4.9}$$

Substitution into Equation 4.7 and rearranging gives

$$I_b(t) + R_a C_g \frac{dI_b(t)}{dt} = GI_t(t) + R_a C_g \frac{dI_t(t)}{dt} \tag{4.10}$$

Taking the Laplace transform,

$$I_b(s) + R_a C_g I_b(s)s = GI_t(s) + R_a C_g I_t(s)s \tag{4.11}$$

$$I_b(s)(1 + R_a C_g s) = I_t(s)(G + R_a C_g s) \tag{4.12}$$

The transfer function from thoracic flow to box flow is

$$\frac{I_b(s)}{I_t(s)} = \frac{G + R_a C_g s}{1 + R_a C_g s} \tag{4.13}$$

Then the transfer function from thoracic volume, V_t, to box volume, V_b, is equal to the transfer function from thoracic flow to box flow.

$$\frac{I_b(s)}{I_t(s)} = \frac{s \cdot V_b(s)}{s \cdot V_t(s)} = \frac{V_b(s)}{V_t(s)} = \frac{G + R_a C_g s}{1 + R_a C_g s} \tag{4.14}$$

Since the derivative is inherently noisy, it is more convenient to integrate box flow and use volume signals than to take the derivative of thoracic volume and use flow signals.

Substituting $s = j\omega$:

$$\frac{V_b(j\omega)}{V_t(j\omega)} = \frac{G + j\omega R_a C_g}{1 + j\omega R_a C_g} \tag{4.15}$$

$$\frac{V_b(j\omega)}{V_t(j\omega)} = \frac{G + j\omega R_a C_g}{1 + j\omega R_a C_g} \cdot \frac{1 - j\omega R_a C_g}{1 - j\omega R_a C_g} \tag{4.16}$$

$$\frac{V_b(j\omega)}{V_t(j\omega)} = \frac{G + \omega^2 R_a^2 C_g^2 + j(1 - G)\omega R_a C_g}{1 + \omega^2 R_a^2 C_g^2} \tag{4.17}$$

So the phase angle, θ, between thoracic volume and box volume is given by

$$\tan\theta = \frac{(1 - G)\omega R_a C_g}{G + \omega^2 R_a^2 C_g^2} \tag{4.18}$$

Rearranging

$$\omega^2 \tan\theta (R_a C_g)^2 - \omega(1 - G) R_a C_g + G \tan\theta = 0 \tag{4.19}$$

Solving for $R_a C_g$

$$R_a C_g = \frac{(1 - G) \pm \sqrt{(1 - G)^2 - 4G\tan^2\theta}}{2\omega \tan\theta} \tag{4.20}$$

Only the smaller root of the above equation yields physiologically relevant val-

ues (see APPENDIX).

$$R_a C_g = \frac{(1-G) - \sqrt{(1-G)^2 - 4G\tan^2\theta}}{2\omega\tan\theta} \tag{4.21}$$

Alternately, dropping the higher order term of Equation 4.19 provides reasonable accuracy. This results in the following solution

$$R_a C_g = \frac{G\tan\theta}{2\pi(1-G)f} \tag{4.22}$$

Results presented in this research were calculated using Equation 4.21.

Specific airway resistance

Specific airway resistance is defined as

$$sRaw = R_a \cdot TGV \tag{4.23}$$

where TGV is thoracic gas volume. Gas compliance in the lung (assuming isothermal conditions) can be written as

$$C_g = \frac{TGV}{P_{atm} - P_{H2Oa}} \tag{4.24}$$

By substitution of Equation 4.24 into Equation 4.23, it is seen that specific airway resistance is the time constant R_aC_g multiplied by pressure $P_{atm} - P_{H2Oa}$:

$$sRaw \equiv R_a \cdot C_g \cdot [P_{atm} - P_{H2Oa}] \tag{4.25}$$

In this research, the measurements were made over a relatively short span of time. Therefore, the pressure term can be considered a constant, and R_aC_g is then a direct measure of specific airway resistance. In this study, estimates of R_aC_g have units given in milliseconds. However, if sRaw is estimated based on $P_{atm} - P_{H2Oa} \approx 1000 \ \ cm\, H_2O$, then from Equation 4.25

$$sRaw = R_aC_g \ \ msec \ \ \cdot 1000 \ \ cm\, H_2O \tag{4.26}$$

$$= 1000 \cdot R_aC_g \ \ cm\, H_2O \cdot msec \tag{4.27}$$

$$= R_aC_g \ \ cm\, H_2O \cdot sec \tag{4.28}$$

Under these conditions, sRaw in units of $cm\, H_2O \cdot sec$ will have the same numerical value as R_aC_g in units of $msec$.

Experimental Design

Six, 21.0 gram (SD 1.7), specific pathogen-free female A/J mice (Jackson Laboratory) were housed in an AAALAC-accredited animal facility at $23\,^{\circ}$C and 50% humidity with a 12 hour light/dark cycle, and were provided standard laboratory mouse chow and tap water *ad libitum*. Each mouse was placed in a chamber for a two minute exposure to aerosolized methacholine chloride dissolved in saline (0, 5, 10 , and 20 mg/mL). Three minutes after exposure, the mice were

transferred to the acoustic plethysmograph for two minutes where box flow and thoracic volume were measured at a sampling rate of $2000\ Hz$. Since all six mice were tested at each concentration prior to increasing to the next concentration of methacholine, the time between doses for each mouse was approximately 45 minutes. All animal procedures were performed in accordance with an animal protocol approved by the NIOSH institutional animal care and use committee.

Statistics

All experimental data (mean $\pm$ SE) were analyzed using one-way ANOVA followed by *post hoc* analysis using Fisher's PLSD [10]. Log transformation was applied to equalize variance between doses. Dose-response trends were determined using regression analysis. Differences were considered significant at $p < 0.05$.

4.1.3 Signal Processing

The electro-mechanical delay between the pressure transducer and the microphone was assessed by lightly tapping the nozzle opening with no animal in the chamber. This produced a pressure drop across the screen while simultaneously interrupting the acoustic signal measured by the microphone. These data were used to calculate the phase shift produced by the electromechanical properties of the transducers, which was subsequently subtracted from the phase shift measured with the animal present in the plethysmograph.

The animal data was processed as follows. A 15 Hz low-pass filter was applied to the data for noise reduction. Box flow was integrated to get box volume. The data were broken into six second segments with a 50% overlap. That is, the first segment is from $t = 0$ seconds to $t = 6$ seconds; the second segment from $t = 3$ seconds to $t = 9$ seconds; etc. An estimate of the transfer function

was computed using Welch's averaged periodogram method [39] (Matlab "tfe" function) with a 4000-point transform size, a 4000-point window, and an overlap of 2000 samples. Using these same parameters, an estimate of the coherence was determined for each segment.

For each segment, the angle of the transfer function was determined at the breathing frequency by linear interpolation from the estimate above. This angle and breathing frequency were used with equation 4.21 to calculate an estimate of R_aC_g for each segment. Similarly, coherence for each segment was determined at the breathing frequency. The mean R_aC_g value was found by averaging the estimates for all the segments whose coherence was greater than or equal to 0.9.

4.2 Results

The results of the methacholine aerosol exposure are shown in Figures 4.7–4.12. At the 5 and 10 mg/mL doses, five of the six mice had elevated R_aC_g compared to baseline (Figure 4.7). At the highest methacholine dose ($20\ mg/mL$), each mouse had an increased R_aC_g compared to saline. The mean R_aC_g dose-response curve is shown in Figure 4.8. The mean increase from baseline for 5 and 10 mg/mL doses was $57\,\%$ and $61\,\%$, respectively. At the $20\ mg/mL$ dose, the mean increase was over $227\,\%$, or a little more than a tripling of R_aC_g.

The airway resistance-compliance values were calculated based on the phase shift and the breathing frequency. The results for these two component measurements are shown in Figures 4.9–4.12. In general, there is a dose dependent increase in phase shift, accompanied by a decrease in breathing frequency at the highest dose.

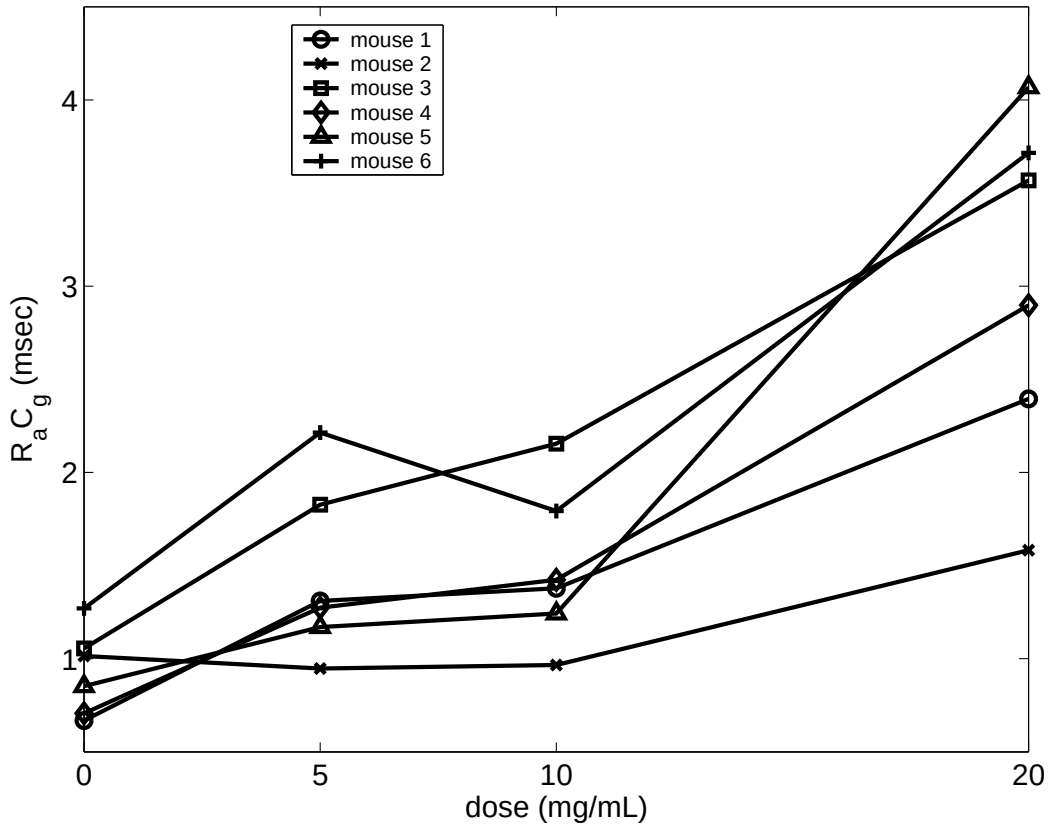

Figure 4.7: Individual R_aC_g dose-response results of the methacholine aerosol exposure.

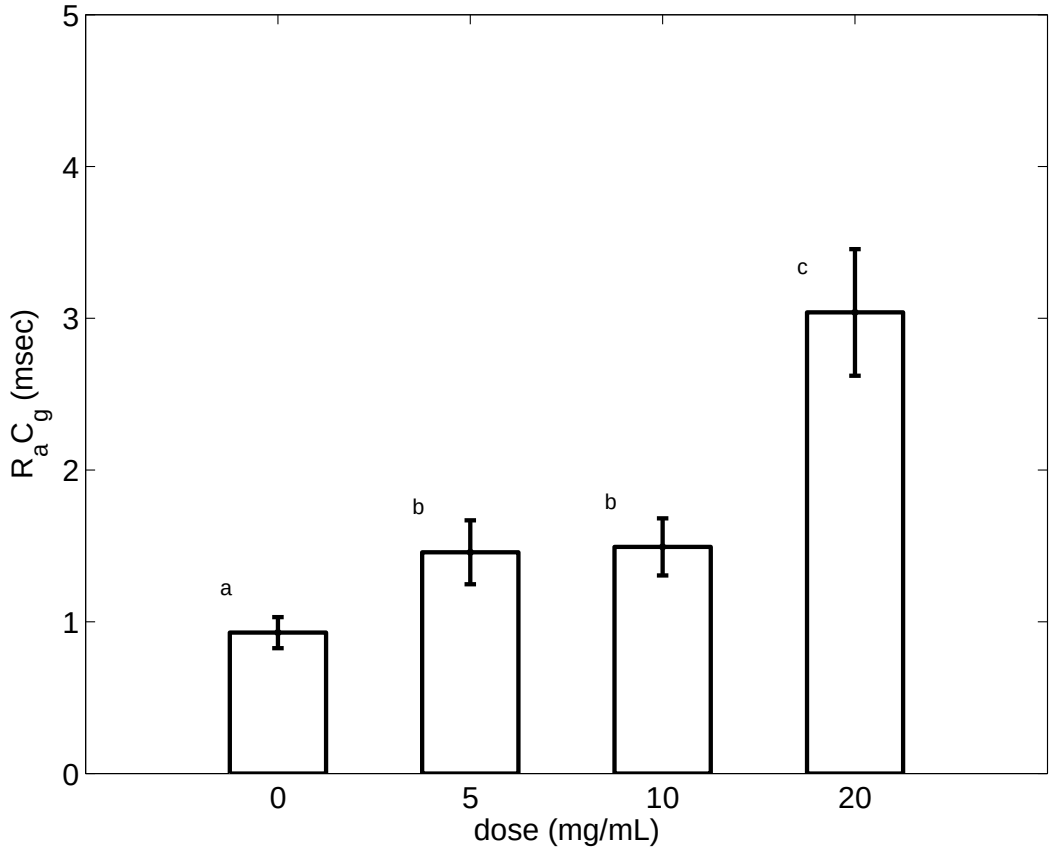

Figure 4.8: Average R_aC_g dose-response results (mean $\pm$ SE) of the methacholine aerosol exposure. Lowercase letters denote statistically significant differences.

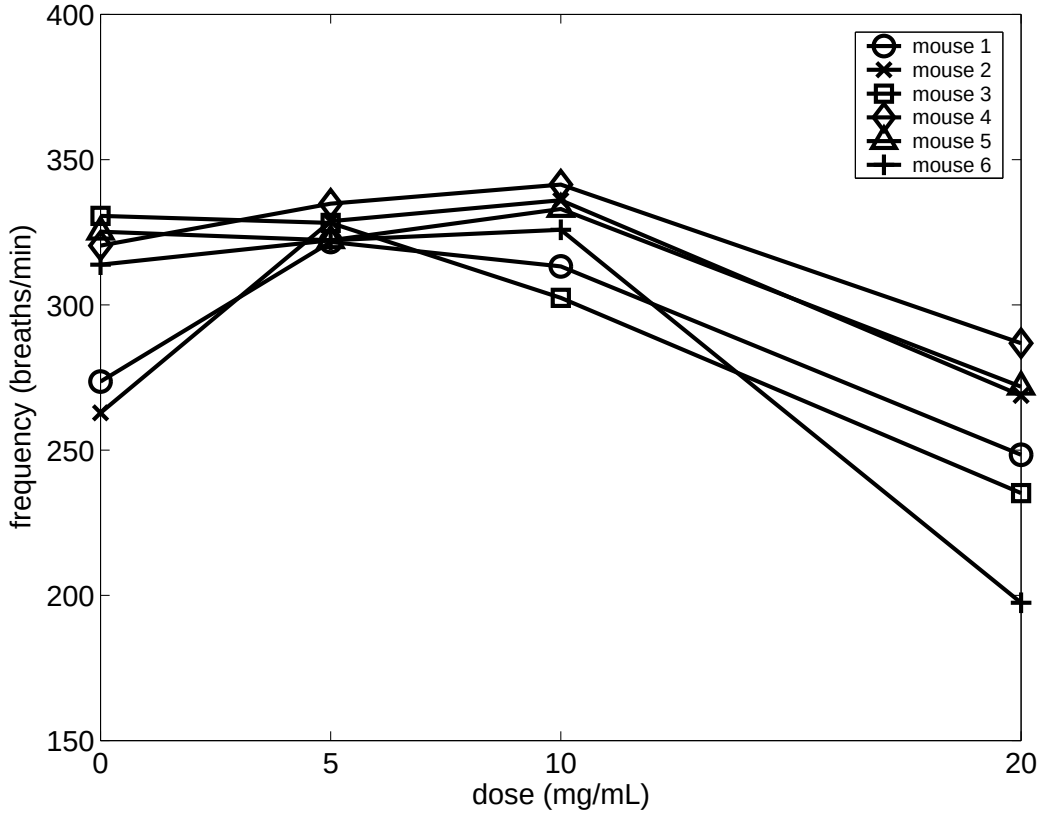

Figure 4.9: Individual breathing frequency dose-response results of the methacholine aerosol exposure.

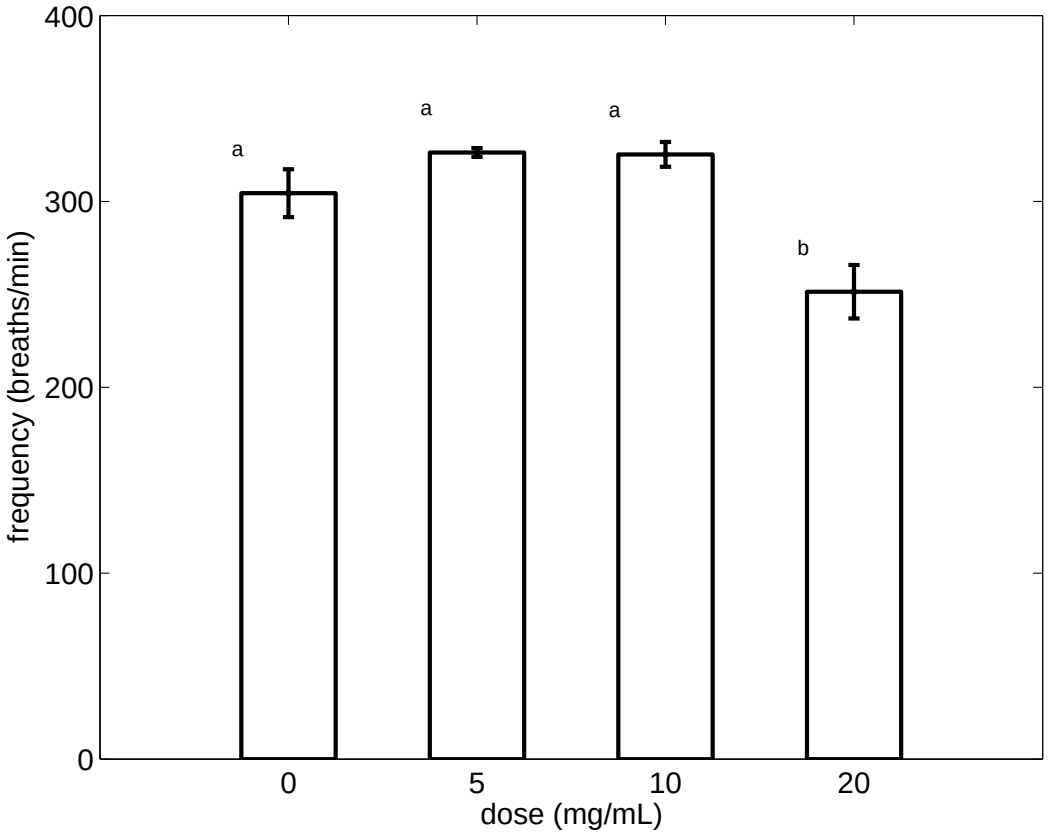

Figure 4.10: Average breathing frequency dose-response results (mean $\pm$ SE) of the methacholine aerosol exposure. Lowercase letters denote statistically significant differences.

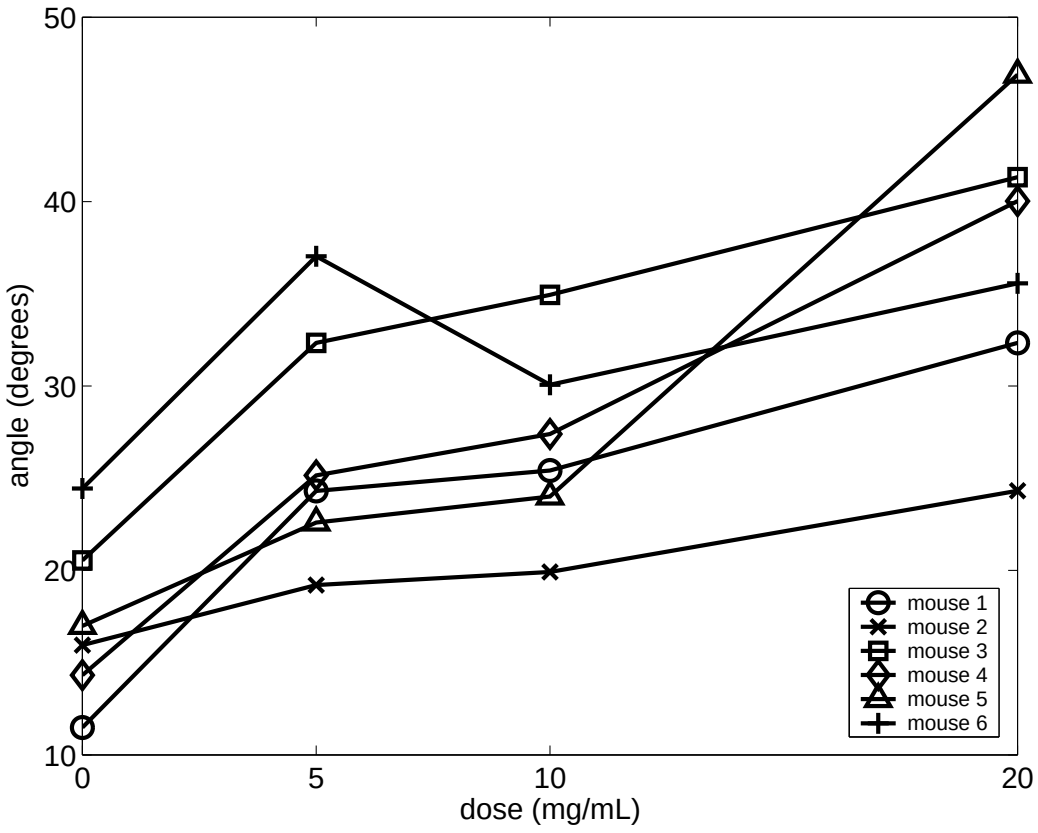

Figure 4.11: Individual phase shift dose-response results of the methacholine aerosol exposure.

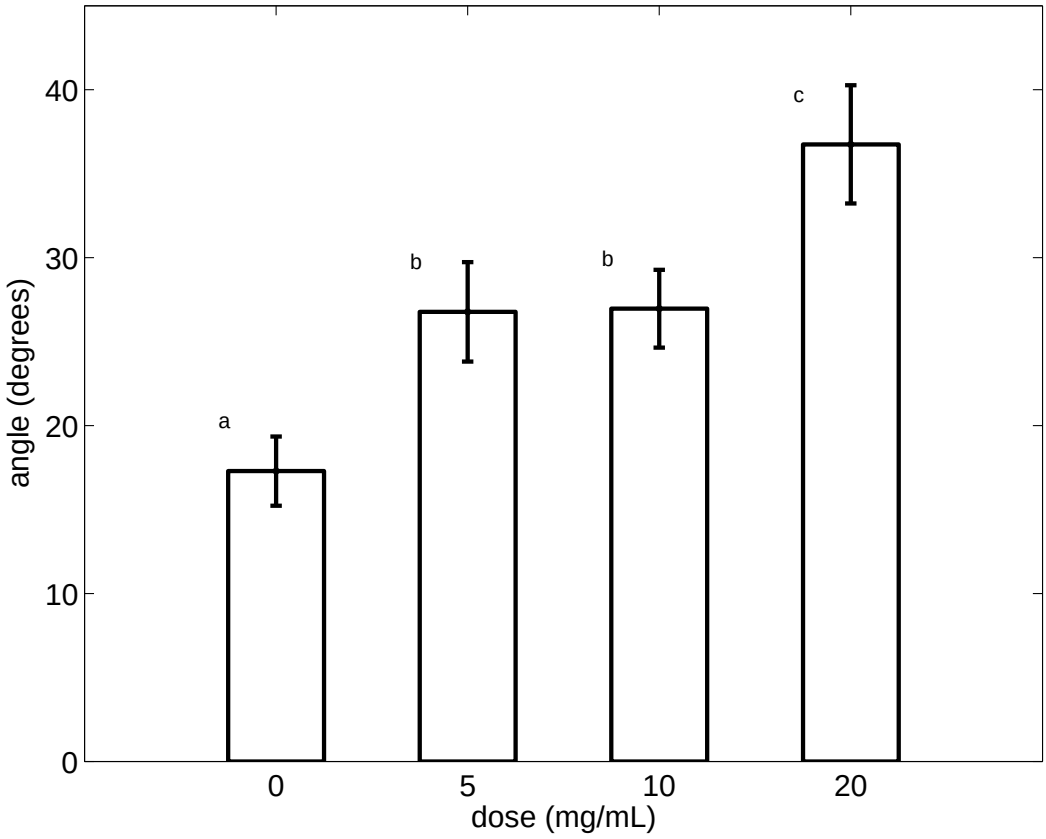

Figure 4.12: Average phase shift dose-response results (mean $\pm$ SE) of the methacholine aerosol exposure. Lowercase letters denote statistically significant differences.

Chapter 5

Discussion

5.1 Discussion

The signal measured from a spontaneously respiring animal in the traditional whole-body plethysmograph is generated from the thoracic flow of the animal filtered by the mechanical properties of the airways. Therefore, changes in this signal can result either from changes in the thoracic flow pattern or from changes in the respiratory "filter." The drawback of past methods utilizing the unrestrained plethysmograph is that in order to relate changes in the filter (i.e. specific airway resistance, etc.) based solely on changes in the WBP signal, it must be assumed that the thoracic flow pattern is unchanged. Likewise, to relate tidal volume to changes in the WBP signal, it must be assumed that thoracic gas compression is negligible. The plethysmograph presented in this research overcame this issue by allowing measurement of the thoracic flow signal in addition to the WBP signal. This allows assessment of R_aC_g even in cases where the breathing pattern of the animal is significantly affected. It also allows measurement of tidal volume nearly independent of gas compression.

In the first part of this research, the idea of using a resonating cavity to mea-

sure changes in mouse volume was explored. The use of a resonating cavity to measure volume has been used in the past to design an infant plethysmograph for static body volume measurements [9, 8, 38]. By manually changing the frequency to measure the resonance of the plethysmograph with a subject inside, and comparing this to the resonance of an empty chamber, they were able to measure average body volume. Jimenez, et. al [24] later designed a modified and improved acoustic plethysmograph. No attempt, however, was made to track the resonant frequency as a function of time to measure tidal volume in either system. In contrast, we present a system that operates at a fixed frequency, and automatically tracks the change in sound amplitude as a function of time due to change in animal volume.

In the second part of this research, a modified plethysmograph was presented that allows estimation of sRaw. The baseline specific airway resistance value of $0.93 \pm 0.10\ cm\ H_2O \cdot sec$ obtained in this research is consistent with previously reported baseline values in A/J mice. Lofgren, et al. [37] found baseline sRaw of $0.676 \pm 0.027\ cm\ H_2O \cdot sec$ in A/J mice using a restrained whole-body plethysmograph. However, in a direct comparison of systems using BALB/c mice, they found that sRaw determined in their restrained whole-body plethysmograph was about one third the value they measured using a double chamber plethysmograph. Delorme and Moss [7] measured sRaw in A/J mice using a double chamber plethysmograph. In two trials performed a minimum of two days apart, they found values of $1.68 \pm 0.06\ cm\ H_2O \cdot sec$ and $1.49 \pm 0.14\ cm\ H_2O \cdot sec$. Additionally, our baseline results are nearly identical to those of Flandre, et al. [18] for BALB/c and C57BL/6 mice measured using a double chamber plethysmograph.

Direct comparison of dose-response curves is inexact since the actual delivered dose is affected by the specific nebulizer, airflow, tubing arrangement, etc. However, there is general agreement in our results and those of Lofgren, et al. [37], particularly at the highest dose used, where sRaw was elevated and the breathing frequency was depressed.

The acoustic plethysmograph presented in this research has some limitations.

First, the system is sensitive to noise generated at or near the excitation frequency in the room and by the animal in the chamber. The room noise can be abated by placing the plethysmograph inside a box lined with acoustic foam during testing. Band pass filtering the output signal prior to demodulation further reduces the effects of external noise and reduces noise generated by the animal.

The AWBP output voltage curve is highly sensitive to the excitation frequency. It is important to use a generator with a stable output over the length of the testing period. In our system, the function generator exhibited a slight frequency drift over a period of hours. This small drift produced a shift in the output curve. Since we calibrated daily, this did not present a problem, but if the shift had occurred during a test, a corresponding change in the DC level of the output voltage would have been observed. Although small deviations in frequency produced shifts in the output curve, the slope of the curve at the operation point remained nearly identical. Thus, the calibration is not changed, but a DC shift in output voltage is observed.

Motion of the animal in the chamber also produced some artifact in the output voltage. Small movements and animal grooming did not produce any observable distortions. Large animal movement tended to produce a shift in the DC level of the signal. One possible explanation is that the placement of the animal affects the radiation resistance of the nozzle. Small changes in resistance would produce slights shifts in the output curve. As in the case with excitation frequency, it is unlikely the calibration would be affected, but a shift in the DC signal level would be observed. The animal restrainer is designed to keep the animal from affecting the nozzle resistance, but it may be too close in the prototype system. However, the acoustic plethysmograph appears to be much less sensitive to animal motion compared to the traditional whole body plethysmograph.

The addition of a screen to the plethysmograph nozzle adds significant acoustic resistance to the system. This in turn reduces volume sensitivity. This reduction in sensitivity complicates calibration of the volume signal and allows significant

noise degradation of the volume measurement. On the other hand, a higher screen resistance increases the sensitivity and noise immunity of box pressure measurements. The ideal solution (and future improvement) would be a device for measuring nozzle flow that has little flow resistance.

Although a low resistance flow meter would be ideal, the method presented in this research allows us to overcome the shortcomings of measuring flow with a screen pneumotach. We have presented a method of estimating R_aC_g that is dependent only on the phase of the transfer function. As described in the Appendix, using only phase does limit the range of measurable R_aC_g. The ability to use magnitude and phase information over a range of frequencies is desirable and would likely remove these limitations. However, the limits of R_aC_g using phase are high enough that they are likely irrelevant for assessing the pulmonary response of the mouse in most cases. Because we are only using phase, it is not necessary to calibrate the thoracic volume or the box volume signal since the magnitude is unimportant. Furthermore, even in the presence of significant noise on the thoracic volume signal, we are able to measure the increase in specific airway resistance due to methacholine exposure using only the phase information.

The purpose of this research was to develop a system for measuring pulmonary function in conscious, unrestrained mice. The lack of, and need for, such a system has been well documented (see for example [31, 30]). Attempts to develop methods for measuring pulmonary function parameters, derived from the single pressure measurement in the WBP, and related to airway resistance in conscious, unrestrained animals have been going on for at least a decade [22, 19, 26, 27]. More recently, as the empirical parameter Penh has fallen out of favor [1], efforts in this regard have intensified. During the same period that this research was conducted, scientists have developed systems with the similar goal of making an additional measurement from the unrestrained plethysmograph. Lai-fook et al. [25] used x-rays to measure end-expiratory and tidal volumes in conscious mice, while Bates et al. [3] developed a system using video to estimate tidal volume. However, these systems appear to be much less practical [30] than the one presented here. Indeed, the developer of the

video-assisted plethysmograph system has commented on the elegance of the acoustic approach [2]. Additionally, to my knowledge, no one other than the developers of these systems has put the x-ray or video-assisted approaches into practice, whereas the acoustic approach [36] has already been adopted in a system for measuring tidal volume in neonatal mice [6].

In summary, an acoustic whole body plethysmograph has been developed capable of measuring pulmonary function in mice. The system uses a single frequency excitation of a resonant cavity to measure change in volume of the mouse. This measure, along with the traditional plethysmograph pressure, allow estimates of tidal volume and specific airway resistance in conscious, unrestrained animals.

Bibliography

[1] J. Bates, C. Irvin, V. Brusasco, J. Drazen, J. Fredberg, S. Loring, D. Eidelman, M. Ludwig, P. Macklem, J. Martin, J. Milic-Emili, Z. Hantos, R. Hyatt, S. Lai-Fook, A. Leff, J. Solway, K. Lutchen, B. Suki, W. Mitzner, P. Pare, N. Pride, and P. Sly. The use and misuse of penh in animal models of lung disease. *Am J Respir Cell Mol Biol*, 31:373–374, 2004.

[2] J. H. T. Bates. Faculty of 1000 Biology, 2 Jun 2008 http://www.f1000biology.com/article/id/1108982/evaluation.

[3] J. H. T. Bates, J. Thompson-Figueroa, L. K. A. Lundblad, and C. G. Irvin. Unrestrained video-assisted plethysmography: a noninvasive method for assessment of lung mechanical function in small animals. *J Appl Physiol*, 104:253–261, 2008.

[4] D. T. Blackstock. *Fundamentals of Physical Acoustics*. John Wiley and Sons, Inc., New York, 2000.

[5] Schmid W. D. Temperature gradients in the nasal passage of some small mammals. *Comp Biochem Physiol*, 54A:304–308, 1975.

[6] J. A. Daubenspeck, A. Li, and E. E. Nattie. Acoustic plethysmography measures breathing in unrestrained neonatal mice. *JAP*, 104:262–268, 2008.

[7] M. P. DeLorme and O. R. Moss. Pulmonary function assessment by whole-body plethysmography in restrained versus unrestrained mice. *J Pharmacol Toxicol Methods*, 47:1–10, 2002.

[8] W. G. Deskins, D. C. Winter, H. P. Sheng, and C. Garza. An acoustic plethysmograph to measure total infant body volume. *J. Biomech. Eng.*, 107(4):304–308, 1985.

[9] W. G. Deskins, D. C. Winter, H. P. Sheng, and C. Garza. Use of a resonating cavity to measure body volume. *J. Acoust. Soc. Am.*, 77(2):756–758, 1985.

[10] S. Dowdy, W. Wearden, and D. Chilko. *Statistics for Research*, pages 283–285. John Wiley and Sons, Inc., third edition, 2004.

[11] J. M. Drazen, P. W. Finn, and G. T. De Sanctis. Mouse models of airway responsiveness: physiological basis of observed outcomes and analysis of selected examples using these outcome indicators. *Annu Rev Physiol*, 61:593–625, 1999.

[12] J. E. Drorbaugh and W. O. Fenn. A barometric method for measuring ventilation in newborn infants. *Pediatrics*, 16:81–87, 1955.

[13] A. B. DuBois, A. W. Brody, D. H. Lewis, and B. F. Jr. Burgess. Oscillation mechanics of lungs and chest in man. *J. Appl. Physiol.*, 8:587–594, 1956.

[14] G. Enhorning, S. van Schaik, C. Lundgren, and I. Vargas. Whole-body plethymography, does it measure tidal volume in small animals? *Can. J. Physiol. Pharmacol.*, 76:945–951, 1989.

[15] M. A. Epstein and R. A. Epstein. A theoretical analysis of the barometric method for measurements of tidal volume. *Respir Physiol*, 32:105–120, 1978.

[16] R. A. Epstein, M. A. Epstein, G. G. Haddad, and R. B. Mellins. Practical implementation of the barometric method for measurement of tidal volume. *J Appl Physiol*, 49(6):1107–15, 1980.

[17] R. R. Fay. Comparative psychoacoustics. *Hearing Research*, 34:295–306, 1988.

[18] T. D. Flandre, P. L. Leroy, and D. J. M. Desmecht. Effect of somatic growth, strain, and sex on double-chamber plethymographic respiratory function values in healthy mice. *J. Appl. Physiol.*, 94:1129–1136, 2003.

[19] D. G. Frazer, A. A. Afshari, W.T. Goldsmith, N. Phillips, and V. A. Robinson. Estimation of guinea pig airway resistance following exposure to cotton dust measured with a whole body plethysmograph. In R. R. Jacobs and P. J. Wakelyn, editors, *Proceedings of the Twenty-First Cotton and Organic Dust Research Conference*, volume 12, pages 171–174, 1997.

[20] M. R. Gamble. Sound and its significance for laboratory animals. *Biol. Rev.*, 57:395–421, 1982.

[21] R. F. M. Gomes, X. Shen, R. Ramchandani, R. S. Tepper, and J. H. T. Bates. Comparative respiratory system mechanics in rondents. *J Appl Physiol*, 89:908–16., 2000.

[22] E. Hamelmann, J. Schwarze, K. Takeda, A. Oshiba, G. L. Larsen, C. G. Irvin, and E. W. Gelfand. Noninvasive measurement of airway responsiveness in allergic mice using barometric plethysmography [see comments]. *Am J Respir Crit Care Med*, 156(3 Pt 1):766–75, 1997.

[23] J. P. Jacky. Barometric measurement of tidal volumes: effects of pattern and nasal temperature. *J. Appl. Physiol.*, 49(2):319–325, 1980.

[24] O. S. V. Jiminez, J. K. Moon, C. L. Jensen, F. A. Vohra, and H. P. Sheng. Pre-term infant volume measurements by acoustic plethysmography. *J. Biomed. Eng.*, 15:91–98, 1993.

[25] S. J. Lai-Fook, P. K. Houtz, and Y. Lai. End-expiratory and tidal volumes measured in conscious mice using single projection x-ray images. *J. Appl. Physiol.*, 104:521–533, 2008.

[26] S. J. Lai-Fook and Y. Lai. Airway resistance due to alveolar gas compression measured by barometric plethysmography in mice. *J. Appl. Physiol.*, 98:2204–2218, 2005.

[27] Lennart K. A. Lundblad, Charles G. Irvin, Andy Adler, and Jason H. T. Bates. A reevaluation of the validity of unrestrained plethysmography in mice. *J. Appl. Physiol.*, 93:1198–1207, 2002.

[28] R. G. Lyons. *Understanding Digital Signal Processing*. Prentice Hall, second edition, 2004.

[29] Lomask M. Further exploration of the penh parameter. *Exp Toxicol Pathol*, 57(S2):13–20, 2006.

[30] W. Mitzner. Why can't mice just learn to pant? *J. Appl. Physiol.*, 105:402, 2008.

[31] W. Mitzner, C. Tankersley, L. K. A. Lundblad, C. G. Irvin, A. Adler, and J. H. T. Bates. Interpreting penh in mice. *J. Appl. Physiol.*, 94(2):828–832, 2003.

[32] H. F. Olson. *Acoustical Engineering*, chapter 5. Professional Audio Journals, Inc., 1991.

[33] B. E. Pennock, C. P. Cox, R. M. Rogers, W. A. Cain, and J. H. Wells. A noninvasive technique for measurement of changes in specific airway resistance. *J. Appl. Physiol.*, 46(2):399–406, 1979.

[34] R. Peslin, C. Duvivier, M. Vassiliou, and C. Gallina. Thermal artifacts in plethysmographic airway resistance measurements. *J. Appl. Physiol.*, 79(6):1958–1965, 1995.

[35] R. Peslin, P. Jardin, and B. Hannhart. Modeling of the relationship between volume variations at the mouth and chest. *J. Appl. Physiol.*, 41(5):659–667, 1976.

[36] J.S. Reynolds and D.G. Frazer. Unrestrained acoustic plethysmograph for measuring tidal volume in mice. *Ann Biomed Eng*, 34(9):1494–1499, 2006.

[37] Lofgren L. S., M. R. Mazan, E. P. Ingenito, K Lascola, M Seavey, A Walsh, and A. M. Hoffman. Restrained whole body plethysmography for measure of strain-specific and allergen induced airway responsiveness in conscious mice. *J. Appl. Physiol.*, 101:1495–1505, 2006.

[38] H. P. Sheng, A. L. Adolph, E. O. Smith, and C. Garza. Body volume and fat-free mass determinations by acoustic plethysmography. *Pediatr. Res.*, 24(1):85–89, 1988.

[39] R. Shiavi. *Introduction to applied statistical signal analyis*, pages 259–260. Academic Press, second edition, 1999.

[40] E. E. Sinnett, A. C. Jackson, D. E. Leith, and J. P. Butler. Fast integrated flow plethysmograph for small mammals. *J Appl Physiol*, 50(5):1104–1110, 1981.

Appendix

In order to infer specific airway resistance from the phase shift of the transfer function given in Equation 4.17, Equation 4.19 must be solved for R_aC_g. Since Equation 4.19 is quadratic in R_aC_g, the phase angle, θ, initially increases with an increase in R_aC_g, but eventually reaches a peak and then decreases as R_aC_g continues to increase. As a result, there are two solutions for any given phase shift. Figure 5.1 displays the phase angle versus airway resistance-compliance for the model at two frequencies and $G = 0.1$. A reasonable approach is to use only the portion of the curve that is monotonically increasing (that is, the smaller of the two solutions).

It can be shown that the value of the peak angle is constant for a constant G. However, the phase angle reaches a peak at a lower R_aC_g as frequency increases. The curve denoting the peak angle (which is constant for constant G) as a function of frequency and R_aC_g is shown in Figure 5.2. Given the breathing frequency, this curve defines the maximum R_aC_g that can be inferred from the phase angle. As an example, consider a mouse breathing at $5\ Hz$. As the animal's airways constrict, the phase angle would increase until R_aC_g reaches approximately $10\ msec$. As the airways continue to narrow, the phase would begin to drop, appearing as though R_aC_g were actually decreasing. However, since the R_aC_g for normal mice is approximately $1\ msec$, it would appear to be an extreme case for R_aC_g to cross the limit shown in Figure 5.2. Even for a mouse breathing at the unusually high frequency of $10\ Hz$, airway resistance-compliance could quintuple before the limit would be reached.

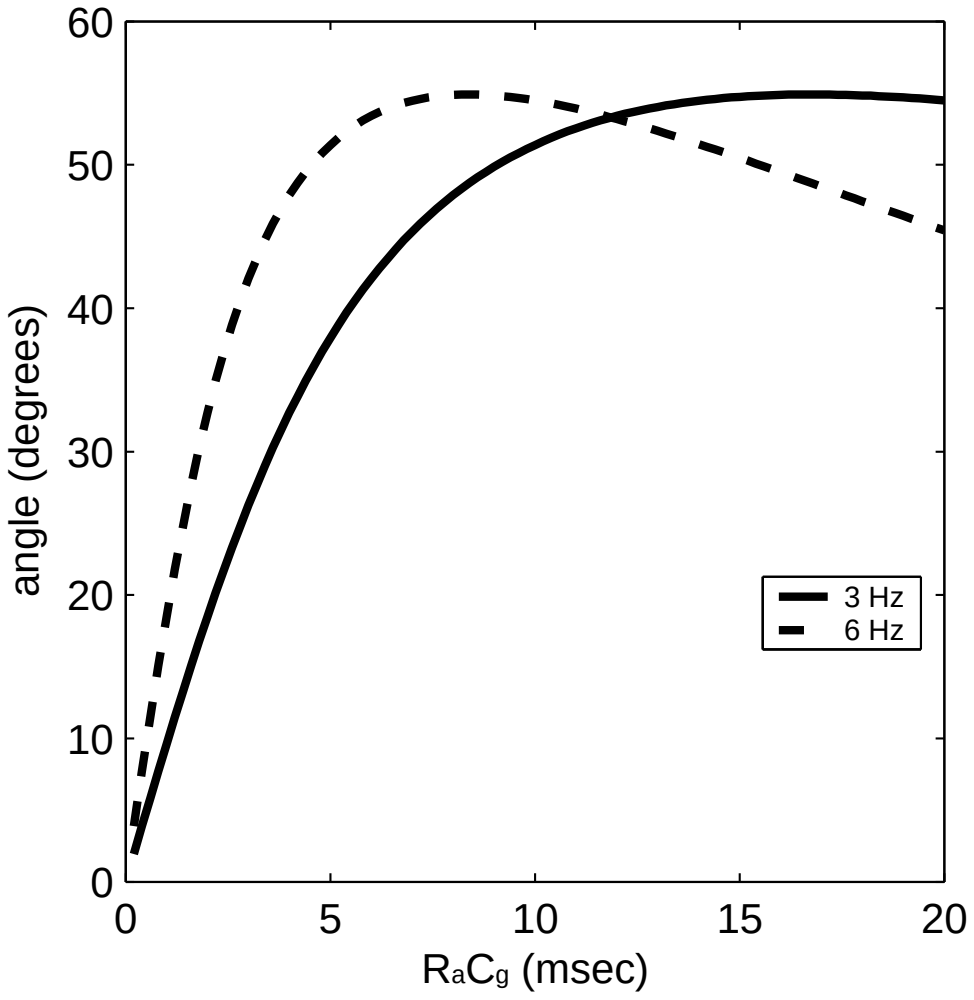

Figure 5.1: These curves represent the theoretical phase response, as a function of R_aC_g, of the model for two frequencies.

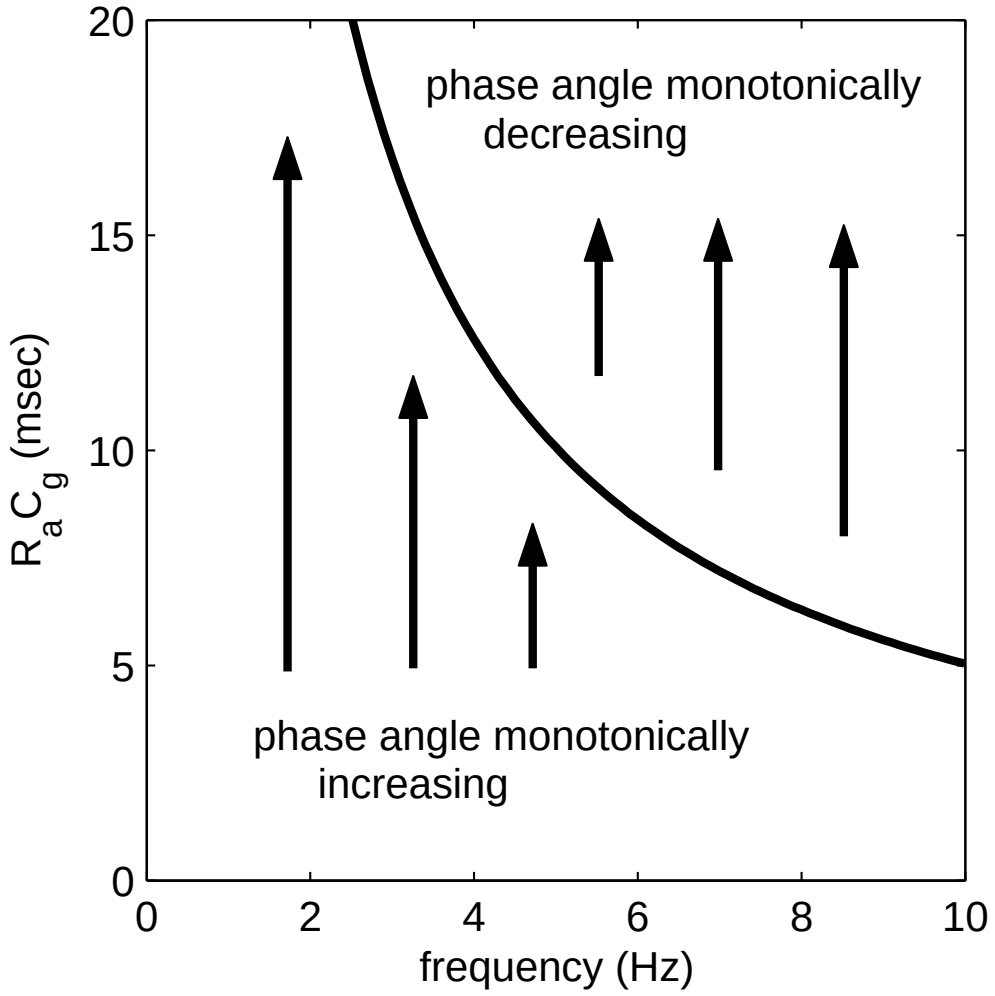

Figure 5.2: For any given frequency, the model phase shift increases monotonically with R_aC_g up to a maximum phase (denoted by the line) after which the phase angle decreases.

Finally, for $f = 5\ Hz$, Figure 5.3 displays R_aC_g as a function of the phase angle for Equations 4.21 and 4.22. The simplified expression of Equation 4.22 produces a slight underestimation of R_aC_g. For assessing mice whose R_aC_g is in the range of normal to $300\,\%$ of normal, Equation 4.22 provides reasonable accuracy.

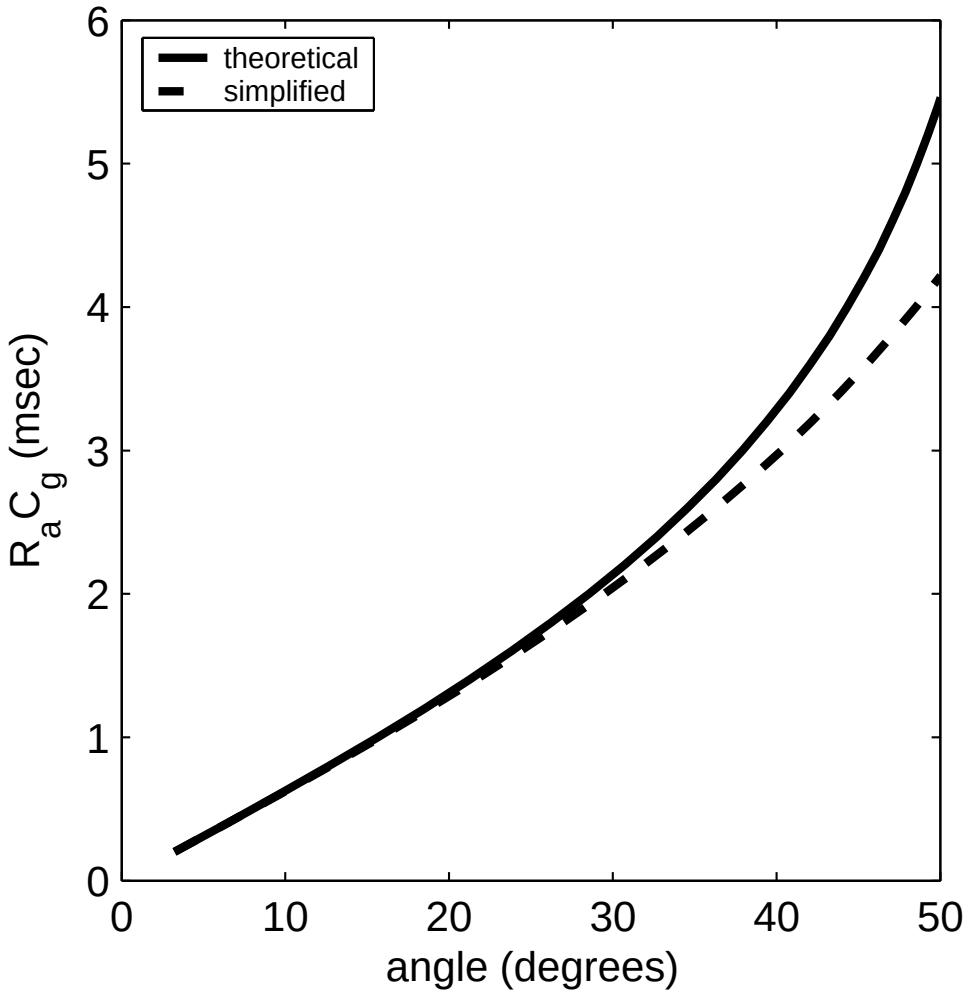

Figure 5.3: $R_a C_g$ as predicted from the model phase shift at a frequency of $5\ Hz$. The solid line represents the exact solution (Equation 4.21). The dashed line represents the solution to the simplified expression (Equation 4.22).